J. Fluid Mech. (2008), *vol.* 603, *pp.* 1–38.
doi:10.1017/S0022112008000578 Printed in the United Kingdom

Viscous and inviscid centre modes in the linear stability of vortices: the vicinity of the neutral curves

DAVID FABRE[1] AND STÉPHANE LE DIZÈS[2]

[1]IMFT, allée du professeur Soula, 31400 Toulouse, France

[2]IRPHE-CNRS, 49 rue F. Joliot-Curie, F-13013 Marseille, France

(Received 27 April 2007 and in revised form 11 January 2008)

In a previous paper, we have demonstrated that if the Reynolds number is sufficiently large, all trailing vortices with non-zero rotation rate and non-constant axial velocity become linearly unstable with respect to a class of viscous centre modes. We provided an asymptotic description of these modes which applies away from the neutral curves in the (q, k)-plane, where q is the swirl number which compares the azimuthal and axial velocities, and k is the axial wavenumber. In this paper, we complete the asymptotic description of these modes for general vortex flows by considering the vicinity of the neutral curves. Five different regions of the neutral curves are successively considered. In each region, the stability equations are reduced to a generic form which is solved numerically. The study permits us to predict the location of all branches of the neutral curve (except for a portion of the upper neutral curve where it is shown that near-neutral modes are not centre modes). We also show that four other families of centre modes exist in the vicinity of the neutral curves. Two of them are viscous damped modes and were also previously described. The third family corresponds to stable modes of an inviscid nature which exist outside of the unstable region. The modes of the fourth family are also of an inviscid nature, but their structure is singular owing to the presence of a critical point. These modes are unstable, but much less amplified than unstable viscous centre modes. It is observed that in all the regions of the neutral curve, the five families of centre modes exchange their identity in a very intricate way. For the q vortex model, the asymptotic results are compared to numerical results, and a good agreement is demonstrated for all the regions of the neutral curve. Finally, the case of 'pure vortices' without axial flow is also considered in a similar way. In this case, centre modes exist only in the long-wave limit, and are always stable. A comparison with numerical results is performed for the Lamb–Oseen vortex.

1. Introduction

The stability of trailing vortices with respect to normal mode disturbances is a matter of interest for various applications, such as, for example, the dynamics and dispersal of aircraft trailing wakes. The mapping of the various kinds of waves and instabilities existing in such flows have occupied workers for several decades. In this paper, we focus on particular eigenmodes called *centre modes* because they are strongly concentrated in the vicinity of the vortex axis.

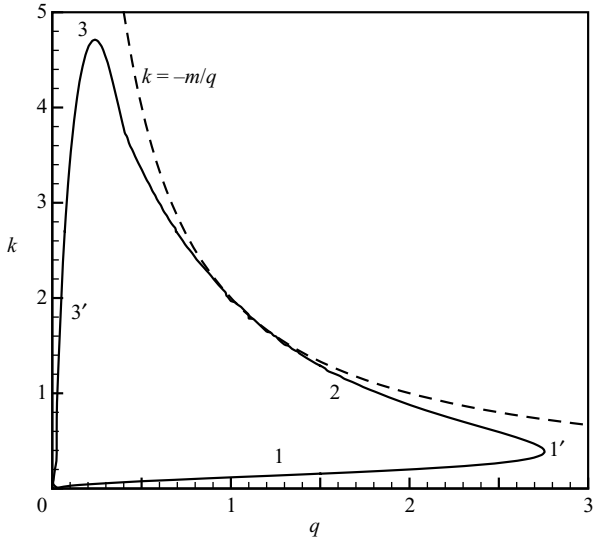

FIGURE 1. The typical shape of the unstable region for viscous centre modes in the q-vortex. The vicinity of the neutral curve is divided into five regions denoted 1, 1′, 2, 3, 3′ (see text).

The existence of centre modes of either a viscous or an inviscid nature has been reported in several numerical and asymptotic studies. Two base flows have received particular attention. First, a systematic study of these centre modes in the case of the swirling Poiseuille flow was conducted by Stewartson, Ng & Brown (1988, hereinafter referred to as SNB). They investigated two regions corresponding to the vicinity of the neutral curves in a Reynolds number/swirl number diagram, and demonstrated the existence of unstable centre modes in these regions. They showed that the most amplified modes are of a viscous nature and gave a description of these modes with a multiple scale analysis. They also showed that these modes coexist with modes of a second kind which are inviscid at leading order but are singular owing to the presence of a critical layer for some real value of r.

The second base flow which was particularly considered is the q-vortex model (often called Batchelor's vortex, though it is actually a simplification of Batchelor's (1964) non-parallel trailing-vortex solution). Until recently, it was generally believed that instabilities exist in this flow only for values of the swirl number q smaller that 1.5. Some recent studies have changed this view. First, Fabre & Jacquin (2004, hereinafter referred to as FJ) have shown that unstable viscous centre modes, related to those existing in the swirling Poiseuille flow, are actually present in this model for all values of q if the Reynolds number is sufficiently large. Figure 1 shows the typical shape of the instability region in the plane defined by the axial wavenumber k and the swirl number q, for negative values of the azimuthal wavenumber m. The instability region is contained within the domain bounded by the hyperbola of equation $k = -m/q$ and the axes of equations $k = 0$ and $q = 0$. As the Reynolds number tends to infinity, the instability domain tends to fill this region completely.

Le Dizès & Fabre (2007, hereinafter referred to as LDF) subsequently provided an asymptotic description of these modes in the large-Reynolds-number limit. This study is conducted in a general framework and extends the results obtained by SNB for the swirling Poiseuille flow. For the q-vortex, the analysis shows that the frequencies of

the unstable modes are given by the following expression:

$$\omega = mq + k + 3\mathrm{e}^{\mathrm{i}\pi/6}|kq(kq+m)|^{1/3}Re^{-1/3} + (n+1/2)\mathrm{e}^{-\mathrm{i}\pi/4}|6(mq+2k)|^{1/2}Re^{-1/2} \quad (n=0,1,2,\ldots). \tag{1.1}$$

(This formula is valid for $k < -mq/2$; otherwise a slightly different form has to be employed.) The unstable modes following this formula were called 'viscous modes of kind A' by LDF. They also showed that, in addition to these unstable modes, there exist two other families of damped viscous centre modes called viscous modes of kinds B and C. The frequencies of these modes are also given by (1.1), for certain complex choices of the cubic root. Modes of kind B exist in the same region as the unstable modes A, as described in figure 1, and modes of kind C exist outside of this region. The prediction of LDF was successfully compared to numerical results for the q-vortex for all kinds of modes. However, their description cannot be used in the vicinity of the neutral curves. Inspection shows that in this case the terms of order $Re^{-1/3}$ and $Re^{-1/2}$ become comparable in magnitude, so the asymptotic expansion is no longer correctly ordered. The study of these degenerated regions constitutes the primary objective of this paper.

Apart from the viscous modes just discussed, the q-vortex also possesses eigenmodes of an inviscid nature, and some of them occasionally acquire a centre-mode behaviour. First, unstable inviscid modes exist inside the domain depicted in figure 1. These modes form an infinite family indexed by an integer n. The precise region of existence of these modes was obtained by Heaton (2007) who showed that, unlike what was generally believed, this region extends up to $q = 2.31$. Heaton (2007) also showed that the higher modes of this family display a centre-mode behaviour when the index n becomes large, all the other parameters remaining of order one. It can be noted that these modes also become centre modes in another limit, namely for large values $|m|$ and in the regions $q \approx -mk/2$ and $q \approx \sqrt{2}$ (Stewartson & Leibovich 1987).

A second category of modes with an inviscid nature is formed by the Kelvin waves, which are neutral modes with a real frequency. Such waves were described for the q-vortex by Le Dizès & Lacaze (2005), and they generally exist outside of the domain of existence of the viscous modes displayed in figure 1. Leibovich, Brown & Patel (1986, referred to as LBP hereinafter), found that some of these waves behave as centre modes on the external sides of the curves of equation $k = 0$ and $k = -m/q$ bounding the domain of viscous modes in figure 1. Therefore, the curves defined by $k = 0$, $k = -m/q$ and $q = 0$ delimit the regions of existence of several families of centre modes with either a viscous or an inviscid nature, and interactions between these families can be anticipated in their vicinity. One of the objectives of this paper is to clarify the relations between all these families of centre modes.

Finally, both viscous and inviscid centre modes also exist in 'pure' vortices without axial flow. This was demonstrated, in particular, in the numerical study of Fabre, Sipp & Jacquin (2006) for the Lamb–Oseen vortex. The description of the centre modes in this case constitutes the third objective of this paper.

The procedure used here differs from that of LDF for several aspects. First, LDF directly consider the limit $Re \to \infty$ in the primitive equations with all the other parameters remaining of order one. Here we will consider a distinguished limit, where some parameter (such as the wavenumber or the swirl number) approaches zero as the Reynolds number tends to infinity. Secondly, in LDF, the structure of the eigenmodes is formed of four imbricated layers which have to be matched with each other, whereas in our case the structure of the eigenmode is contained within a single

region. Finally, in LDF, the resolution is made almost entirely in an analytic way. Here, on the other hand, we generally end up with a system of equations which has to be solved numerically. The whole procedure is close to what was performed in §§ 3 and 4 of SNB for the swirling Poiseuille flow, and the results of SNB are recovered as particular cases of our work.

As in LDF, all the analyses will be conducted in the general case in terms of the Taylor coefficients of the base flow at the centre. However, the general form of the unstable domain given in figure 1 for the q-vortex remains valid in the general case if the swirl number is defined in a convenient way.

Turning back to figure 1, the neutral curve can be divided into five regions, whose successive study constitutes the summary of this paper (after a general presentation of the base flows and stability equations in § 2).

Region 1 is the region of the 'lower neutral curve', and is considered in § 3.
Region 1′ is the region of the critical swirl number q_c, and is considered in § 4.
Region 2 is the region of the 'upper neutral curve', and is considered in § 5.
Region 3 is the region of the critical wavenumber k_c, and is considered in § 6.1.
Region 3′ is the region of the 'left neutral curve', and is considered in § 6.2.

A comparison of these asymptotic predictions with a numerical solution of the full problem in the case of a q-vortex is postponed to § 7. The case of a pure vortex (without axial velocity) is then considered in § 8, and comparisons are made with the numerical results of Fabre *et al.* (2006) for a Lamb–Oseen vortex. Conclusions are given in § 9. Finally, the Appendices regroup analytical developments relevant to some particular limits of the cases treated in the main text.

2. Base flow and stability equations

2.1. *Base flows*

A columnar vortex is characterized by its angular velocity field $\Omega(r) = V(r)/r$ and its axial velocity field $W(r)$. The asymptotic analyses conducted in this paper do not depend on the complete base flow, but only on its properties in the vicinity of the vortex axis. Consequently, we will consider a general base flow defined by its Taylor expansion around the axis, with the following form:

$$\Omega(r) = \Omega_0 + \frac{\Omega_2 r^2}{2} + O(r^4), \tag{2.1}$$

$$W(r) = W_0 + \frac{W_2 r^2}{2} + \frac{W_4 r^4}{24} + O(r^6). \tag{2.2}$$

The terms Ω_0, Ω_2, W_0, W_2, W_4 are assumed to be non-dimensionalized in a proper way by the definition of length and velocity scales. Viscous effects are characterized by a Reynolds number $Re = 1/\nu$, where the viscosity ν is non-dimensionalized using the same scales. For example, for trailing vortices, the usual choice is to define the velocity scale as the difference of axial velocity between the vortex centre and the outer flow, and the length scale as the dispersion radius of axial vorticity. However, other choices of scales are possible and may be more convenient in other contexts. So, as in LDF, we prefer not to favour a particular flow and leave the scalings unspecified.

In the present study, we will generally assume that $\Omega_0 > 0$, $\Omega_2 \leqslant 0$ and $W_2 \leqslant 0$. These assumptions mean that both the axial velocity and the rotation rate (and, therefore, also the axial vorticity) are maximum at the vortex centre. However, most of the analysis can easily be adapted for other signs of the parameters by symmetry considerations.

It is usual to introduce a swirl number, q, which compares the scales of the azimuthal and axial velocities. In the general case where the velocities are given by their Taylor expansions, there are several ways to define such a parameter. Here, we will define the swirl number in the following way:

$$q = \frac{-2\Omega_0}{W_2}. \tag{2.3}$$

For this definition, the 'upper neutral curve' will always lie in the vicinity of the hyperbola of the equation $k = -m/q$, whatever the precise vortex model.

For comparison with available work, three specific base flows will be particularly considered. The first one is the q-vortex model, used in most studies on trailing vortices (see e.g., FJ), defined by

$$\Omega(r) = q\frac{1-\exp(-r^2)}{r^2}, \quad W(r) = \exp(-r^2). \tag{2.4}$$

In this case, we have $\Omega_0 = q$, $\Omega_2 = -q$, $W_0 = 1$, $W_2 = -2$, $W_4 = 12$, and the swirl number defined by (2.3) is obviously consistent.

The second particular base flow is the swirling Poiseuille flow, considered in particular by SNB, defined (for $r < 1$) by

$$\Omega(r) = 1, \quad W(r) = \epsilon(1-r^2). \tag{2.5}$$

In this case, we have $\Omega_0 = 1$, $\Omega_2 = 0$, $W_0 = \epsilon$, $W_2 = -2\epsilon$, $W_4 = 0$. The parameter ϵ is the Rossby number related to the inverse of the swirl number ($q = \epsilon^{-1}$).

Finally, the third particular base flow is the Lamb–Oseen vortex, whose eigenmodes were mapped by Fabre *et al.* (2006), defined by

$$\Omega(r) = \frac{1-\exp(-r^2)}{r^2}, \quad W(r) = 0. \tag{2.6}$$

This latter case corresponds to $\Omega_0 = 1$, $\Omega_2 = -1$, $W_0 = W_2 = W_4 = 0$.

2.2. *Stability equations*

In the stability analysis we consider infinitesimal disturbances in the form of eigenmodes, characterized by an axial wavenumber k, an azimuthal wavenumber m, and a complex frequency ω, i.e.

$$(u'_r, u'_\theta, u'_z, p') = [u(r), v(r), w(r), p(r)]\exp(\mathrm{i}kz + \mathrm{i}m\theta - \mathrm{i}\omega t). \tag{2.7}$$

Linearizing the continuity and momentum equations leads to the following set of equations:

$$\frac{1}{r}\frac{\partial}{\partial r}(ru) + \frac{\mathrm{i}m}{r}v + \mathrm{i}kw = 0, \tag{2.8a}$$

$$\mathrm{i}(m\Omega + kW - \omega)u - 2\Omega v + \frac{\partial p}{\partial r} = \frac{1}{Re}\left[\left(\Delta_{m,k} - \frac{1}{r^2}\right)u - \frac{2\mathrm{i}m}{r^2}v\right], \tag{2.8b}$$

$$\mathrm{i}(m\Omega + kW - \omega)v + \Xi u + \frac{\mathrm{i}m}{r}p = \frac{1}{Re}\left[\left(\Delta_{m,k} - \frac{1}{r^2}\right)v + \frac{2\mathrm{i}m}{r^2}u\right], \tag{2.8c}$$

$$\mathrm{i}(m\Omega + kW - \omega)w + \frac{\partial W}{\partial r}u + \mathrm{i}kp = \frac{1}{Re}\Delta_{m,k}w. \tag{2.8d}$$

In these equations, $\Xi(r)$ is the base flow axial vorticity, and $\Delta_{m,k}$ is the Laplacian operator, defined, respectively, as

$$\Xi(r) = \frac{1}{r}\frac{\partial}{\partial r}(r^2\Omega(r)), \tag{2.9}$$

$$\Delta_{m,k} = \frac{\partial^2}{\partial r^2} + \frac{1}{r}\frac{\partial}{\partial r} - k^2 - \frac{m^2}{r^2}. \tag{2.10}$$

In addition to the eigencomponents u, v, w, p, our asymptotic derivations will often make use of the axial vorticity component ξ of the eigenmode, defined by

$$\xi = \frac{\partial v}{\partial r} - \frac{\mathrm{i}mu}{r}. \tag{2.11}$$

The linearized equation for ξ is the following:

$$(\mathrm{i}m\Omega + \mathrm{i}kW - \omega)\xi + \frac{\partial \Xi}{\partial r}u = \Xi \mathrm{i}kw - \frac{\partial W}{\partial r}\mathrm{i}kv + \frac{1}{Re}\Delta_{m,k}\xi. \tag{2.12}$$

This equation is obtained by combining (2.8*b*) and (2.8*c*).

3. The long-wave centre modes

3.1. *Asymptotic scalings and equations*

We first focus on the long-wave range ($k \approx 0$). Inspection shows that centre modes are always present in this limit for $m \neq 0$, provided that $\Omega_2 \neq 0$, i.e. when the angular velocity field $\Omega(r)$ has a maximum or minimum value at the vortex centre. On the other hand, they do not exist in the swirling Poiseuille flow considered in SNB (1988), where $\Omega(r)$ is constant.

In this section, we will consider trailing vortices with a non-constant axial flow, i.e. with $W_2 \neq 0$ (long-wave centre modes also exist in pure vortices with $W_2 = 0$ and will be considered in § 9). To simplify the derivations, we will also assume that $m < 0$ and $\Omega_2 < 0$. Thanks to the symmetries of the problem, a change of sign of either m or Ω_2 leads to identical results, with simply a change of sign of both k and the real part of ω.

For the asymptotic derivation, we require both k and $\omega - m\Omega_0$ to be of order $Re^{-1/2}$, and we apply the least degeneracy principle in order to determine the scalings which allow us to keep the maximum number of terms in the equations. The base-flow parameters are also incorporated into the scalings in order to eliminate them as much as possible in the final equations. The relevant scalings are the following:

$$r = Re^{-1/4}|\Omega_2|^{-1/4}\underline{r}, \tag{3.1a}$$

$$k = Re^{-1/2}|\Omega_2|^{3/2}\Omega_0^{-1}(-W_2/2)^{-1}\underline{k}, \tag{3.1b}$$

$$\omega = m\Omega_0 + kW_0 + Re^{-1/2}|\Omega_2|^{1/2}\underline{\omega} + O(Re^{-1}), \tag{3.1c}$$

$$u = \underline{u} + O\left(Re^{-1/2}\right), \tag{3.1d}$$

$$v = \underline{v} + O\left(Re^{-1/2}\right), \tag{3.1e}$$

$$w = Re^{1/4}|\Omega_2|^{-3/4}(-W_2/2)\underline{w} + O\left(Re^{-1/4}\right), \tag{3.1f}$$

$$p = Re^{-1/4}\Omega_0|\Omega_2|^{-1/4}\underline{p} + O\left(Re^{-3/4}\right), \tag{3.1g}$$

$$\xi = Re^{1/4}|\Omega_2|^{1/4}\underline{\xi} + O\left(Re^{-1/4}\right). \tag{3.1h}$$

Let us first introduce these scalings into the r and θ momentum equations, (2.8*b*, *c*). The equations reduce, at leading order, to

$$-2\underline{v} + \frac{\partial \underline{p}}{\partial \underline{r}} = 0, \tag{3.2}$$

$$2\underline{u} + \frac{\mathrm{i}m\underline{p}}{\underline{r}} = 0. \tag{3.3}$$

It is instructive to note that the only remaining terms are the Coriolis forces which equilibrate the pressure gradients. This means that, at leading order, the u and v components of the velocity field satisfy the geostrophic balance. Combining these two equations leads to

$$2\underline{\xi} = \Delta_m \underline{p}, \tag{3.4}$$

where the notation Δ_m corresponds to the two-dimensional Laplacian operator in terms of the scaled variable $\underline{r}$, i.e.

$$\Delta_m = \frac{1}{\underline{r}} \frac{\partial}{\partial \underline{r}} \left(\underline{r} \frac{\partial}{\partial \underline{r}} \right) - \frac{m^2}{\underline{r}^2}. \tag{3.5}$$

This equation, which relates the Laplacian of the pressure to the vorticity field, is also characteristic of the geostrophic regime.

Introducing these scalings into the axial velocity and axial vorticity equation leads to a system of coupled differential equations, which are, respectively, second and fourth order:

$$-\mathrm{i}\left(\frac{m\underline{r}^2}{2} + \underline{\omega} \right) \underline{w} = -\mathrm{i}m\underline{p} + \Delta_m \underline{w}, \tag{3.6}$$

$$-\mathrm{i}\left(\frac{m\underline{r}^2}{2} + \underline{\omega} \right) \Delta_m \underline{p} = -4\mathrm{i}m\underline{p} + 4\mathrm{i}\underline{k}\underline{w} + \Delta_m^2 \underline{p}. \tag{3.7}$$

Furthermore, these two equations can be combined into a single, sixth-order differential equation with the following form:

$$\left(\frac{m\underline{r}^2}{2} + \underline{\omega} - \mathrm{i}\Delta_m \right) \left[\left(\frac{m\underline{r}^2}{2} + \underline{\omega} - \mathrm{i}\Delta_m \right) \Delta_m - 4m \right] \underline{p} + 4\underline{k}m\underline{p} = 0. \tag{3.8}$$

This equation contains the problem in the most compact form. However, it is nonlinear in $\underline{\omega}$, and therefore not suitable for a resolution using a global eigenvalue method. In practice, we have solved the pair of equations (3.6)–(3.7), which is linear in ω, with a Chebyshev collocation method similar to that used by FJ and Fabre *et al.* (2006).

At this stage, we should point out that, through the asymptotic scalings, we have been able to remove all references to the base flow characteristics. Therefore, the results derived in this section are universal and can be applied to all vortex models, provided that the coefficients Ω_0, Ω_2 and W_2 are non-zero constants.

In order to check whether this is a well-posed eigenvalue problem, we have to consider the behaviour of the solutions at $\underline{r} = 0$ and at $\underline{r} = \infty$. At the origin ($r = 0$), the use of axisymmetric coordinates leads to a regular singularity. Trying a Taylor expansion, it is found that three independent regular solutions can be constructed. The three other independent solutions are singular and have to be removed. Now, at $\underline{r} \to \infty$, the problem admits an irregular singularity. Using standard methods (Bender & Orszag 1978), six independent solutions can be constructed, with the following

behaviours : $\underline{r}^{\alpha_0}$, $\underline{r}^{-\alpha_0}$, $\exp(\beta_0\underline{r}^2)$ (twice), and $\exp(-\beta_0\underline{r}^2)$ (twice). The parameters α_0 and β_0 are defined as follows:

$$\alpha_0^2 = m^2 + 8, \quad \beta_0^2 = -\mathrm{i}m/8. \tag{3.9}$$

The two first solutions are algebraic and correspond to 'inviscid' solutions because they could also be derived from the corresponding inviscid problem, obtained by neglecting the Laplacian in the first two brackets. The four other solutions are 'viscous' solutions with exponential behaviour. Among these six solutions, three of them are growing functions and have to be discarded. Therefore, the behaviour at $\underline{r} \to \infty$ leads to three boundary conditions. So, the total number of boundary conditions is 6 and is equal to the order of the differential equation, ensuring that the problem is well-posed and admits a countable infinity of eigenmode solutions.

3.2. *The limiting forms for* $|\underline{k}| \gg 1$

Before presenting the numerical solutions of the problem (3.8), we first consider the possible limits for $\underline{k} \to \infty$. In terms of the primitive parameters, this limit corresponds to the case $Re^{-1/2} \ll k \ll 1$. Therefore, results obtained in this case are expected to match with the predictions obtained by first letting $Re \to \infty$ with fixed k, and then letting $k \to 0$. Two kinds of mode can be predicted in this way.

3.2.1. *The viscous limit*

The first kind of mode that can be expected for $\underline{k} \gg 1$ is the viscous centre mode described by LDF. When translated into the current scalings, the frequencies of these modes are given by the following formula:

$$\underline{\omega} \approx 3|m\underline{k}|^{1/3}\mathrm{e}^{\mathrm{i}\gamma} + (n + 1/2)\sqrt{6|m|}\mathrm{e}^{-\mathrm{i}\pi/4} \qquad (n = 0, 1, 2, \ldots). \tag{3.10}$$

As shown by LDF, three families of viscous modes, A, B and C, are predicted by this formula, with different values of the angle γ. Family A exists for $\underline{k} > 0$, and corresponds to $\gamma = \pi/6$. This is the only family which contains unstable modes; the modes of families B and C are all stable. Family B exists for $\underline{k} > 0$ and corresponds to $\gamma = -\pi/2$, and family C exists for $\underline{k} < 0$ and corresponds $\gamma = -\pi/6$.

3.2.2. *The inviscid limit*

Inviscid centre modes are also present in the long-wave limit, and can be expected to provide a limit for $\underline{k} \gg 1$ for the solutions of the problem (3.8). Such inviscid centre modes were initially described in the inviscid case by LBP, who referred to them as 'fast waves' because their phase velocity ω/k tends to infinity as k tends to zero. These modes are treated in Appendix B, where we recover the results of LBP and extend them to include the leading-order effect of viscosity. In terms of the primitive parameters, the frequencies of these modes are given by the following expression:

$$\omega = (m\Omega_0 + kW_0) + \frac{W_2\Omega_0}{2\Omega_2}Ck + \frac{\mathrm{i}}{Re}\frac{2\Omega_2^2}{W_2\Omega_0}\frac{D}{k}, \tag{3.11}$$

where the terms C and D take discrete positive values indexed by an integer $n = 0, 1, 2, \ldots$. The expressions for $C(m, n)$ and $D(m, n)$ are given in Appendix B, and some numerical values are displayed in table 5. Note that when expressed in the current scalings, (3.11) takes a much simpler expression:

$$\underline{\omega} = C\underline{k} + \frac{\mathrm{i}D}{\underline{k}} + O(\underline{k}^{-3}). \tag{3.12}$$

If $\underline{k} < 0$, the leading-order structure of the eigenmodes, noted $\underline{p}^{(0)}$ and given by equations (B 6) and (B 12), is regular for all real values of $\underline{r}$. These modes can be identified as waves propagating along the vortex. The term C can be interpreted as a dimensionless group velocity relative to the frame of the vortex centre. The term D gives the first viscous correction to the frequency of these waves, and leads to a weak damping. The fact that the viscous correction varies as k^{-1} can be explained by noting that as k decreases, the modes becomes increasingly concentrated at the vortex centre. Therefore, the radial gradients are increased, and the effect of viscosity is enhanced. The same observations were made for the long-wave centre modes of the Lamb–Oseen vortex by Fabre *et al.* (2006) (see also § 8 where this case will be reviewed).

The case $\underline{k} > 0$ leads to completely different conclusions regarding the structure of the modes. In effect, in that case the leading-order structure of the eigenmodes $\underline{p}^{(0)}$, obtained from the inviscid equations, is singular for some real value of $\underline{r}$, noted $\underline{r}_c$ and called the critical point. Eigenmodes with such a structure will be referred to as *inviscid singular modes* in the following. They do not constitute acceptable solutions of the strictly inviscid problem, and were discarded by LBP who concluded that there are no inviscid centre modes for $\underline{k} > 0$. On the other hand, they still provide a possible limit for modes computed using the viscous equations, and it will be shown in the next section that they are effectively reached in this way. Note that (3.11) predicts that in the presence of viscosity, these modes become slightly unstable (although they are always much less amplified than the viscous modes considered previously).

Additional details on the structure of the inviscid modes are given in Appendix B. The relation between these modes and other kinds of inviscid centre modes, in particular those investigated in Heaton (2007), remains to be clarified. We may also wonder if, when moving far away from the $k = 0$ limit, these modes remain singular or if they become regular. These issues will be considered in § 7.4 for the case of the q-vortex.

3.3. *Numerical results*

We now present the numerical solutions $\underline{\omega}(\underline{k}, m)$ of the eigenvalue problem (3.6), (3.7), and compare the results to the various limiting cases considered above. We restrict ourselves to the case $m = -1$. The results for $m = -2$ and $m = -3$ show similar trends and are available as a supplement to the online version of the paper.

Numerical results for $m = -1$ are shown in figure 2 with thick lines. The dashed lines correspond to the 'inviscid' predictions derived in § 3.2 (equation (3.12) with the values of C and D taken in table 1). The dotted lines correspond to the results for the three families of viscous modes A, B and C predicted by (3.10). As can be observed, all of the predicted limits for $|\underline{k}| \to \infty$ are being attained by some numerical branch. The accordance with the asymptotic limits is good for all kinds of branches, although it requires larger values of $|\underline{k}|$ for the inviscid branches than for the viscous branches.

The figure shows that the various kinds of branches exchange their identity in the long-wave region in a very intricate way. This exchange occurs in two places. First, for $\underline{k} \approx 0$, the branches separate into two subsets, the first leading to unstable modes of both viscous modes of kind A and inviscid singular modes, and the second leading to stable viscous modes of kind B. Secondly, for positive and substantially large values of $\underline{k}$, 'crossing events' occur when one unstable branch, initially following the 'viscous A' behaviour, crosses the next branch and acquires the 'inviscid singular' behaviour. In figure 2, such an event takes place for $\underline{k} \approx 40$, giving rise to the first branch of 'inviscid singular' modes. Similar events occur outside of the range of the figure and give rise

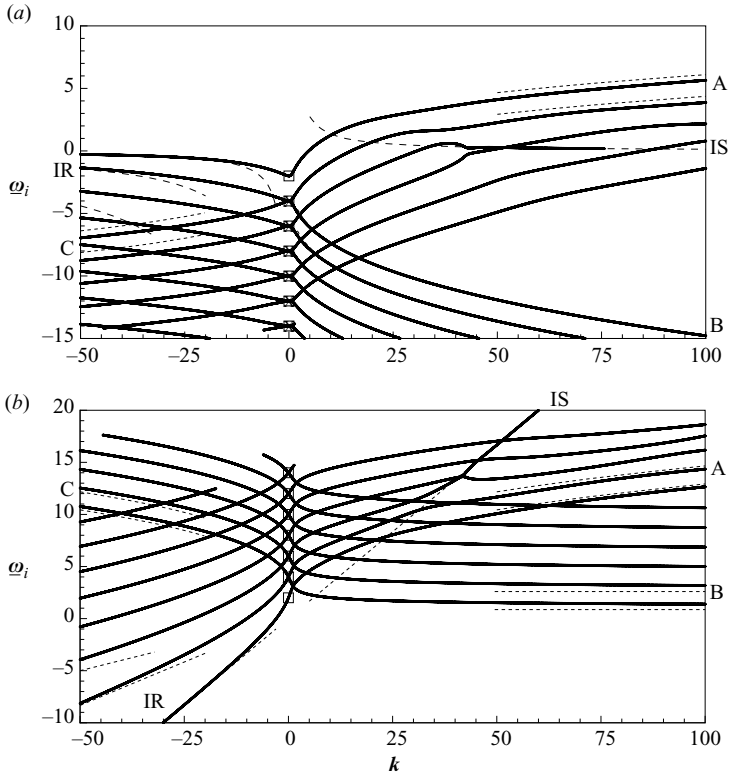

FIGURE 2. Asymptotic results for long-wave centre modes for $m=-1$. (*a*) Imaginary part and (*b*) real part of the frequencies $\underline{\omega}$. Numerical results are shown by solid lines. Inviscid limits for $\underline{k}\gg 1$ are displayed with dashed lines and are labelled IR and IS (for regular and singular behaviours) Viscous limits for $\underline{k}\gg 1$ are shown by dotted lines and are labelled A, B, C. The symbols represent two-dimensional results for 'w' modes (upward-pointing triangles) and 'p' modes (downward-pointing triangles).

m	$\underline{k}_c$	$\underline{\omega}_c$	A_c
−1	4.730	4.514	0.1408
−2	12.962	8.088	0.1142
−3	29.862	12.1726	0.0858

TABLE 1. Values of the lower neutral point $\underline{k}_c$, the corresponding frequency $\underline{\omega}_c$ and the term A_c defined in (4.6) (for $m=-1,-2,-3$).

to the higher branches of this family. This mode-crossing phenomenon has already been observed in the numerical study of the q-vortex by FJ, and in the asymptotic study of the swirling Poiseuille flow by SNB. As we will see in the following sections of the present paper, this feature occurs in the vicinity of all the neutral curves.

The results in the two-dimensional case ($\underline{k}=0$) are also shown in figure 2 by symbols. This case is treated in Appendix A, where it is shown that there are two distinct series of modes, with frequencies given, respectively, by (A 5) and (A 6). The first ones (downward-pointing triangles in figure 2) are called w-modes because they only have an axial velocity component. The second ones (upward-pointing triangles

in figure 2) are called p-modes because only the pressure component is significant. Note that for $|m|=1$, the w- and p-modes correspond to the same frequencies (except the first w-mode which is alone). This degeneracy does not occur for other values of m.

For the mapping of the neutral curves, the most important result is the value $\underline{k}_c$ corresponding to the destabilization of the first branch. These values, and the corresponding values of the frequency $\underline{\omega}_c$, are given in table 1 for $m=-1, -2$ and -3. It is important to point out that the values of $\underline{k}_c$ are universal and do not depend upon the precise base flow. Therefore, for all kinds of vortices, the lower neutral curve will always be given by

$$k_{lower} = Re^{-1/2}|\Omega_2|^{3/2}\Omega_0^{-1}(-W_2/2)^{-1}\underline{k}_c. \tag{3.13}$$

4. The region of the critical swirl number

In the former section, we have investigated the long-wave regime in the case where the Reynolds number tends to infinity, while the base-flow parameters Ω_0, Ω_2, etc... all remain of order one. In this section, we consider the region of the critical swirl number (region $1'$ in figure 1). In this region, the axial wavenumber is both close to the 'upper neutral curve' defined by $k_{upper} \approx -m/q$ and close to the lower neutral curve defined by $k_{lower} \approx Re^{-1/2}|\Omega_2|^{3/2}\Omega_0^{-1}|W_2/2|^{-1}$. We therefore expect the following parameter

$$A = \left(\frac{k_{upper}}{k_{lower}}\right)^{2/3} = |\Omega_2| Re^{-1/3}\left(\frac{W_2}{2}\right)^{4/3}, \tag{4.1}$$

to be of order 1 in this region.

There are several ways to obtain this condition: for instance, Ω_2 can be large, of order $Re^{1/3}$ with $W_2 = O(1)$, or W_2 can be $O(Re^{-1/4})$ with $\Omega_2 = O(1)$. For the q-vortex, $A = qRe^{-1/3}$, which means that the critical swirl number is $O(Re^{1/3})$ in this case.

The analysis of region $1'$ is similar to the lower neutral curve. The same scalings as introduced in (3.1) can be used. However, to distinguish from the development of the former section, we change the notation and write all scaled quantities with a circumplex instead of an underline, i.e. we write $\hat{r}$ instead of $\underline{r}$, etc... . Note, however, that the formal dependency with respect to the Reynolds number will be different from (3.1). It will also depend on whether W_2 is small or Ω_2 is large.

Repeating the analysis of § 3.1, we see that at leading order, the radial and azimuthal momentum equations still lead to the geostrophic balance (3.3), and that the vorticity equation still leads to (3.7). On the other hand, the axial momentum equation now contains an additional term, and takes the following form:

$$-\mathrm{i}\left(\frac{1}{2}m\hat{r}^2 + \hat{\omega}\right)\hat{w} = -\mathrm{i}\left(m + A^{3/2}\hat{k}\right)\hat{p} + \Delta_m \hat{w}. \tag{4.2}$$

Combining this equation with (3.7) leads to the following single sixth-order differential equation:

$$\left(\tfrac{1}{2}\mathrm{i}m\hat{r}^2 + \mathrm{i}\hat{\omega} + \Delta_m\right)\left[\left(\tfrac{1}{2}\mathrm{i}m\hat{r}^2 + \mathrm{i}\hat{\omega} + \Delta_m\right)\Delta_m - 4\mathrm{i}m\right]\hat{p} = 4\hat{k}\left(m + A^{3/2}\hat{k}\right)\hat{p}. \tag{4.3}$$

It turns out that this equation is identical to (3.8), if we simply do the following substitution:

$$\underline{k} \equiv \hat{k}\left(1 + \frac{A^{3/2}\hat{k}}{m}\right). \tag{4.4}$$

Therefore, the results in the region of the critical swirl number can be directly deduced from those of the long-wave region studied in § 3. In particular, a necessary and sufficient condition for instability is that, for some value of $\hat{k}$, we have

$$\hat{k}\left(1+\frac{A^{3/2}\hat{k}}{m}\right) > \underline{k}_c. \tag{4.5}$$

This latter condition is met if A verifies the following property:

$$A < A_c \quad \text{with } A_c = |m|^{2/3}2^{-4/3}\underline{k}_c^{-2/3}. \tag{4.6}$$

In terms of the base flow parameters, the condition of instability thus reads:

$$|\Omega_2||W_2/2|^{-4/3} < A_c Re^{1/3}\ . \tag{4.7}$$

The numerical values of A_c are displayed in table 1 for $m=-1,-2,-3$. Again, this condition is universal and provides a necessary and sufficient condition of instability with respect to centre modes, whatever the precise vortex base flow.

To apply these results to the case of the q-vortex, we first note that in this case we must use the following scalings:

$$q = ARe^{1/3}, \quad k = Re^{-1/3}A^{1/2}\hat{k}, \quad \omega = mq + k + Re^{-1/3}A^{1/2}\hat{\omega}. \tag{4.8}$$

Thus, the condition of instability is $q < q_c$, with $q_c = A_c Re^{1/3}$. As expected from the numerical simulations (FJ), it is the helical perturbations ($m=-1$) which have the largest critical swirl number:

$$q_c = 0.1408Re^{1/3}. \tag{4.9}$$

The corresponding wavenumber and frequency are:

$$k_c = 3.550Re^{-1/3}, \quad \omega_c = -0.1408Re^{1/3}. \tag{4.10}$$

Note that these results for the q-vortex were reported in de Souza (1998).

5. The region of the upper neutral curve ($k \approx -m/q$)

5.1. *Asymptotic scalings*

We now consider the region of the 'upper neutral curve', i.e. the vicinity of $k \approx -m/q$ (with q given in the general case by (2.3)). As in § 3, we look for the asymptotic scalings which permit us to reduce the equations to a convenient form. We assume that all base-flow parameters Ω_0, Ω_2, W_0, W_2, W_4 (and therefore also the swirl number q) are $O(1)$, and suppose that W_2 is negative and Ω_0 is positive. The scalings are as follows:

$$r = Re^{-1/4}|W_2/2|^{-1/2}\Omega_0^{1/4}\bar{r}, \tag{5.1a}$$

$$k = -m/q + Re^{-1/2}|W_2/2|^2\Omega_0^{-5/2}\bar{k}, \tag{5.1b}$$

$$\omega = m\Omega_0 + kW_0 + Re^{-1/2}|W_2/2|\Omega_0^{-1/2}\bar{\omega} + O(Re^{-1}), \tag{5.1c}$$

$$u = \bar{u}_0 + Re^{-1/2}|W_2/2|\Omega_0^{-3/2}\bar{u}_1 + O(Re^{-1}), \tag{5.1d}$$

$$v = \bar{v}_0 + Re^{-1/2}|W_2/2|\Omega_0^{-3/2}\bar{v}_1 + O(Re^{-1}), \tag{5.1e}$$

$$w = Re^{-1/4}|W_2/2|^{1/2}\Omega_0^{-3/4}\bar{w} + O\left(Re^{-3/4}\right), \tag{5.1f}$$

$$p = Re^{-1/4}|W_2/2|^{-1/2}\Omega_0^{5/4}\bar{p} + Re^{-3/4}|W_2/2|^{1/2}\Omega_0^{-1/4}\bar{p}_1 + O\left(Re^{-5/4}\right), \tag{5.1g}$$

$$\xi = Re^{1/4}|W_2/2|^{1/2}\Omega_0^{-1/4}\bar{\xi} + O\left(Re^{-1/4}\right). \tag{5.1h}$$

Now we inject these scalings into the primitive equations. The radial and azimuthal equations lead, again, to the geostrophic equilibrium:

$$-2\bar{v}_0 + \frac{\partial \bar{p}}{\partial \bar{r}} = 0, \tag{5.2}$$

$$2\bar{u}_0 + \frac{im\bar{p}}{\bar{r}} = 0. \tag{5.3}$$

The axial momentum equation also leads to (5.3) at leading order. As in § 3, these equations also imply the following relation between the axial vorticity and the pressure:

$$2\bar{\xi} = \Delta_m \bar{p}. \tag{5.4}$$

For the next steps of the derivation, we require the equations corresponding to the next order of the radial, azimuthal and axial momentum equations, and also the one obtained from the leading order of the axial vorticity equation. Those equations are as follows:

$$\mathrm{i}\bar{\Sigma}\bar{u}_0 + Q\bar{r}^2\bar{v}_0 - 2\bar{v}_1 + \partial_{\bar{r}}\bar{p}_1 = \left(\Delta_m - \frac{1}{\bar{r}^2}\right)\bar{u}_0 - \frac{2\mathrm{i}m}{\bar{r}^2}\bar{v}_0, \tag{5.5a}$$

$$\mathrm{i}\bar{\Sigma}\bar{v}_0 - 2Q\bar{r}^2\bar{u}_0 + 2\bar{u}_1 + \mathrm{i}m\bar{p}_1/\bar{r} = \left(\Delta_m - \frac{1}{\bar{r}^2}\right)\bar{v}_0 + \frac{2\mathrm{i}m}{\bar{r}^2}\bar{u}_0, \tag{5.5b}$$

$$\mathrm{i}\bar{\Sigma}\bar{w} + 2(Q-L)\bar{r}^3\bar{u}_0 + \mathrm{i}\bar{k}\bar{p} - 2\bar{r}\bar{u}_1 - \mathrm{i}m\bar{p}_1 = \Delta_m\bar{w}, \tag{5.5c}$$

$$\mathrm{i}\bar{\Sigma}\bar{\xi} + 2\mathrm{i}(\bar{w} + \bar{r}\bar{v}_0) - 4Q\bar{r}\bar{u}_0 = \Delta_m\bar{\xi}, \tag{5.5d}$$

where we have introduced the following quantities:

$$\bar{\Sigma} = m(1 - Q/2)\bar{r}^2 - \bar{\omega}, \tag{5.6a}$$

$$Q = \frac{-4\Omega_0\Omega_2}{W_2^2}, \tag{5.6b}$$

$$L = Q + \frac{2W_4\Omega_0^2}{3W_2^3}. \tag{5.6c}$$

The combination $[\bar{r} \times (5.5b) + (5.5c)]$ allows us to eliminate $\bar{p}_1$ and $\bar{u}_1$, and leads to the introduction of a new variable defined as $\bar{w}^* = \bar{w} + \bar{r}\bar{v}_0$. We see, moreover, that this group of terms also appears in the axial vorticity equation (5.5*d*). After a few rearrangements, these two equations lead to the following set of coupled equations:

$$\mathrm{i}\bar{\Sigma}\bar{w}^* + \mathrm{i}L\bar{r}^2\bar{p} + \mathrm{i}\bar{k}\bar{p} = \Delta_m\bar{w}^* - \Delta_m\bar{p}, \tag{5.7a}$$

$$\mathrm{i}\bar{\Sigma}\Delta_m\bar{p} + 4\mathrm{i}mQ\bar{p} + 4\mathrm{i}m\bar{w}^* = \Delta_m^2\bar{p}. \tag{5.7b}$$

These two equations are linear in the frequency $\bar{\omega}$ and have been used for the resolution of the problem in the rest of this section. They can also be combined into a sixth-order differential equation:

$$(\mathrm{i}\bar{\Sigma} - \Delta_m)[(\mathrm{i}\bar{\Sigma} - \Delta_m)\Delta_m - 4\mathrm{i}mQ]\bar{p} + 4mL\bar{r}^2\bar{p} + 4m\bar{k}\bar{p} - 4\mathrm{i}m\Delta_m\bar{p} = 0. \tag{5.8}$$

As in § 3, we have been able to reduce the problem to a single differential equation for the pressure component. However, we can see that the scaling process has been less successful than in the long-wave region, because the equation still contains a reference to the base flow through the two parameters Q and L. Consequently, this equation will have to be solved on a case-by-case basis. Note that for a q-vortex, the base-flow parameters are $Q = q^2$, $L = 0$.

There are two interesting limits. The first one corresponds to the limit $Q \gg 1$. In this case, (5.8) becomes identical to (3.8) obtained in the long-wave region, if we make the substitution $\bar{r} \equiv Q^{-1/4}\underline{r}$, $\bar{\omega} \equiv Q^{-1/2}\underline{\omega}$, $\bar{k} \equiv -Q^{3/2}\underline{k}$. So, in this case, we can apply the results of § 3 directly. The second interesting limit is obtained for $Q = L = 0$. This case applies to the swirling Poiseuille flow, and was considered by SNB in their § 3. In their study, the scaled frequency is called Λ and the parameter corresponding to our $\bar{k}$ is termed μ. It turns out that our equations are equivalent to those of SNB (although very different in form) if we make the transformation $\Lambda = |m|^{-1/2}\bar{\omega}$, and $\mu = -|m|^{-5/2}\bar{k}$.

The case $Q = L = 0$ is also expected to provide the correct description of the 'upper neutral curves' in the limit of small swirl numbers for a general vortex when Ω_2 is not zero (and has the same order of magnitude as Ω_0). However, the condition that the expressions (5.1) remain well-ordered may also impose additional constraints. For instance, for the q-vortex, the present scaling with $Q = L = 0$ will apply only for $Re^{-1/3} \ll q \ll 1$. The cases of very small swirl numbers where this condition is no longer verified will be considered in § 4.

As for the long-wave range, we first check the consistency of this eigenvalue problem by considering the limit conditions at $\bar{r} \to \infty$. As in § 3, we have four 'viscous' solutions with behaviour $\exp(\pm\beta_1\bar{r}^2)$ (two solutions for each sign), and two 'inviscid' solutions with behaviour $\bar{r}^{\pm\alpha_1}$. The parameters α_1 and β_1 are defined as follows:

$$\alpha_1^2 = m^2 + \frac{8Q}{Q-2} + \frac{16L}{m(Q-2)^2}, \quad \beta_1^2 = -\frac{\mathrm{i}m(Q-2)}{8}. \tag{5.9}$$

Among the four viscous solutions (except for the very singular case where $Q = 2$), two are exponentially growing functions and have to be removed, and the others two are exponentially decaying. The leading-order behaviour of the solution at $\bar{r} \approx \infty$ is therefore given by the inviscid solutions, i.e.

$$\bar{p} \approx c_1\bar{r}^{+\alpha_1} + c_2\bar{r}^{-\alpha_1}. \tag{5.10}$$

If $\alpha_1^2 \geqslant 0$, the condition $c_1 = 0$ leads to a decaying solution, thus allowing for the existence of discrete eigenmodes. (When $\alpha_1 = 0$, (5.10) has to be replaced by $\bar{p} \approx c_1 \log(\bar{r}) + c_2$, so the condition $c_1 = 0$ still selects bounded solutions.) On the other hand, it may happen that $\alpha_1^2 < 0$. In such a case, the two roots $\pm\alpha_1$ are both imaginary numbers, so the two inviscid solutions are both oscillating functions at $\bar{r} \approx \infty$, and no condition on c_1 or c_2 can lead to a decaying solution. In this case, it is impossible to construct modes located entirely in the vicinity of the vortex centre.

Therefore, there will be some portions of the 'upper neutral curve' which cannot be described directly by solving (5.8). More specifically, the condition $\alpha_1^2 < 0$ with α_1^2 given by (5.9*b*) defines a 'forbidden interval' $Q \in]Q_c, 2]$. The lower bound of the interval, Q_c, corresponds to the value where α_1, given by (5.9), vanishes. The upper bound is for $Q = 2$ where α_1 is infinite. Note that for $L = 0$, which corresponds to the q-vortex, the lower bound is given by

$$Q_c = 2m^2/(m^2 + 8). \tag{5.11}$$

In the 'forbidden interval', modes existing in the vicinity of the 'upper neutral curves' are not centre modes, but also extend into the outer region. The solution in this range would require a matching with an outer solution, to provide the proper balance between the coefficients c_1, c_2 appearing in (5.10). This has not been undertaken here. Instead, we shall present in § 7 a numerical solution of the full problem for a q-vortex for a value of q falling within the forbidden interval. Note that in the forbidden

interval, the hyperbola $k=-m/q$ also corresponds to the leading order of the upper neutral point for the inviscid instabilities, which are much more amplified than the viscous ones.

5.2. *Limit cases for* $|\bar{k}| \gg 1$

As in § 3, we first consider the possible limits for $|\bar{k}| \gg 1$.

5.2.1. *The viscous limit*

Some of the modes computed with the scaling of the 'upper neutral curves' are expected to match with the viscous centre modes of LDF. When expressed into the current scalings, the prediction of LDF is as follows:

$$\bar{\omega} \approx 3|m\bar{k}|^{1/3} \exp(\mathrm{i}\gamma_a) + (n+1/2)|6m(Q-2)|^{1/2} \exp(\mathrm{i}\gamma_b) \qquad (n=0,1,2,\ldots). \quad (5.12)$$

As in § 3, this formula predicts three families of modes. Families A and B are located on the side $\bar{k}<0$; family C is located on the side $\bar{k}>0$. The angles γ_a and γ_b take different values depending on the sign of $Q-2$. For $Q<2$, γ_a is $\pi/6$ for modes A, $-\pi/2$ for modes B and $-\pi/6$ for modes C, while γ_b is $-\pi/4$ for all modes. For $Q<2$, γ_a is $5\pi/6$ for modes A, $-\pi/2$ for modes B and $-5\pi/6$ for modes C, while γ_b is $-3\pi/4$ for all modes.

5.2.2. *The inviscid limit*

Inviscid centre modes are also present in the vicinity of the 'upper neutral curve', and can be expected to give a limit for the numerical results. This case is studied in Appendix C. It is shown that inviscid centre modes exist only outside of the 'forbidden interval' defined above, and that their frequencies are given by the expansion:

$$\bar{\omega} = C_1\bar{k} + \frac{\mathrm{i}D_1}{\bar{k}} + O(\bar{k}^{-3}). \quad (5.13)$$

Note that when expressed in terms of the primitive variables, we obtain the following expression (which is valid for all signs of Ω_0, Ω_2 and W_2):

$$\omega = m\Omega_0 + kW_0 + \frac{2\Omega_0^2}{W_2}C_1\left(k+\frac{m}{q}\right) + \left(\frac{-W_2}{2\Omega_0}\right)^3 \frac{\mathrm{i}D_1}{Re}\left(k+\frac{m}{q}\right)^{-1}. \quad (5.14)$$

The parameters C_1 and D_1 depend upon the wavenumber m, an index integer $n=0,1,2\ldots$, and also upon the base-flow parameters Q and L. The expressions for $C_1(m,n;Q,L)$ and $D_1(m,n;Q,L)$ are given in Appendix C. The group velocity coefficients C_1 turn out to be positive below the forbidden interval (i.e. for $0<Q\leqslant Q_c$ with Q_c defined by (5.11)), and negative above this interval (i.e. for $Q>2$). On the other hand, the coefficients D_1 are always negative. Therefore, the inviscid modes will be stable for $\bar{k}>0$, and unstable for $\bar{k}<0$.

Note that these inviscid centre modes have already been investigated, in the inviscid framework, by LBP. The leading-order terms in our expressions agree with their result, except that they overlooked the dependence of the results with respect to the fourth derivative of the axial velocity field, which appears in our parameter L. However, they applied their results only to base flows such as the q-vortex where this parameter is zero.

As in the case $k\approx 0$ investigated in § 3.2.2, the inviscid eigenmodes considered here are of a different nature depending on the sign of $\bar{k}$. It is found that the modes are regular for $\bar{k}>0$ and are of the 'inviscid singular' kind for $\bar{k}<0$. It will be shown

in the next section that they effectively provide the leading order of some branches computed from the viscous equations. The link between these modes and those found in other inviscid studies, in particular Stewartson & Brown (1985) and Heaton (2007) will be considered in § 7.4

5.3. *Numerical results*

We now present numerical solutions of the eigenvalue problem (5.8). We restrict ourselves to the case $L=0$, so that the results will apply directly to the q-vortex with $q^2=Q$. Because of the forbidden interval, two ranges of Q have to be considered: the low-swirl range with $Q\in[0,\,Q_c]$ and the high-swirl range with $Q\in]2,\,\infty]$. We will present results for $m=-1$ with three values of Q, two in the lower range and one in the upper range. The case $m=-2$ has also been considered and leads to similar trends; results are available as a supplement to the online version of the paper.

Results for $Q=0$ are shown in figure 3. As mentioned above, this case applies to the swirling Poiseuille flow and was treated by SNB. The corresponding figure in SNB is their figure 3. The results are identical except that, since we are using a global eigenvalue method while SNB used a shooting method, we are able to catch a larger number of branches. Figure 4 shown the results for $Q=Q_c=2/9$. This value corresponds to the lower bound of the 'forbidden interval', but our numerical method is still able to provide a reliable solution in this limit case. Finally, figure 5 displays results with $Q=4$. In all these figures, we have also displayed the expected limits for $|\bar{k}|\to\infty$ with thin dotted and dashed lines, as defined in figure 2.

All these figures display the same general form, and are similar to the results for the long-wave range shown in § 3. We observe three families of branches on the 'unstable side', (which now corresponds to $\bar{k}<0$) and two families on the stable side. Moreover, a good agreement with the expected limits is obtained for both viscous and inviscid types of behaviour. As in the long-wave region, a first reorganization of the branches takes place in the region $\bar{k}\approx 0$ (however, a close inspection shows subtle differences between all the displayed cases and the long-wave case investigated previously, regarding the way the various kinds of branches reconnect together). A second reorganisation occurs under the form of mode-crossing events between the 'inviscid singular' and 'viscous A' branches, occurring for some negative values of $\bar{k}$.

Finally, the upper neutral point is defined by the value $\bar{k}_c$ where the first branch becomes unstable. The value of $\bar{k}_c$ has been computed as a function of Q for $m=-1$ and -2 and results are shown in figure 6 (still with $L=0$). Note that because of the presence of the 'forbidden interval', these curves consist of two branches, the first one for the low-swirl range ($0<Q\leqslant Q_c$) and the other one for the high swirl range ($Q>2$). The particular values of $\bar{k}_c$ for $Q=L=0$ are termed $\bar{k}_{c,0}$ and their numerical values for $m=-1,-2,-3$ are given in table 2 as well as the corresponding frequencies. The value for $m=-1$ is in accordance with the value $\mu_0\approx 3.8$ given by SNB.

In terms of the primitive variables, the 'upper neutral curve' is thus given, in the general case, by

$$k_{upper}=\frac{mW_2}{2\Omega_0}+Re^{-1/2}|W_2/2|^2\Omega_0^{-5/2}\bar{k}_c, \tag{5.15}$$

where $\bar{k}_c$ is, in general, a function of the base-flow parameter Q and L.

m	$\bar{k}_{c,0}$	$\bar{\omega}$
-1	-3.842	4.095
-2	-18.920	9.029
-3	-57.867	14.924

TABLE 2. Numerical values for the upper neutral point $\bar{k}_{c,0}$ for $Q = L = 0$, and the corresponding frequency $\bar{\omega}$ (for $m = -1, -2, -3$).

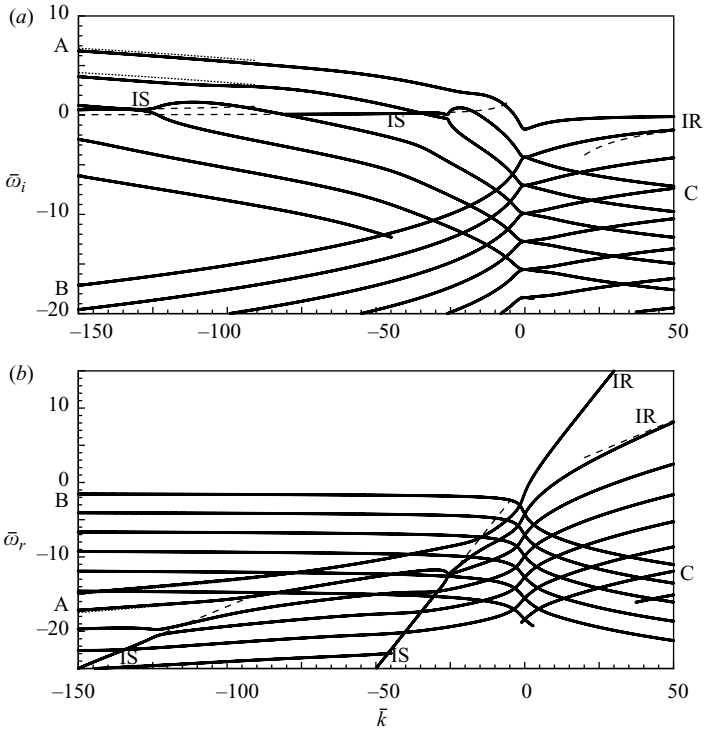

FIGURE 3. Asymptotic results for upper point scalings with $Q = L = 0$, $m = -1$. Details as in figure 2.

6. The regions of small swirl

In the former section, we have investigated the vicinity of the 'upper neutral curve' by letting the Reynolds number tend to infinity and assuming that all base-flow parameters remain of order one. Considering the expressions (5.1*a*)–(5.1*h*), which were the starting point of this analysis, we may observe that these expressions constitute well-ordered developments if the quantity $Re^{-1/2}|W_2/2|\Omega_0^{-3/2}$ is small. In this section, we consider the case where this quantity is of order one or larger. For this purpose, it is convenient to introduce a 'rescaled swirl number', defined as

$$\check{q} = \Omega_0 Re^{1/3}|W_2/2|^{-2/3}. \tag{6.1}$$

The whole analysis of the previous section can thus be re-interpreted as the case $\check{q} \gg 1$. The case $\check{q} = O(1)$ corresponds to the 'critical wavenumber region' (region 3 in figure 1) and will be considered in § 6.1. The case $\check{q} \ll 1$ corresponds to the 'left neutral curve region' (region 3′ in figure 1) and will be considered in § 6.2.

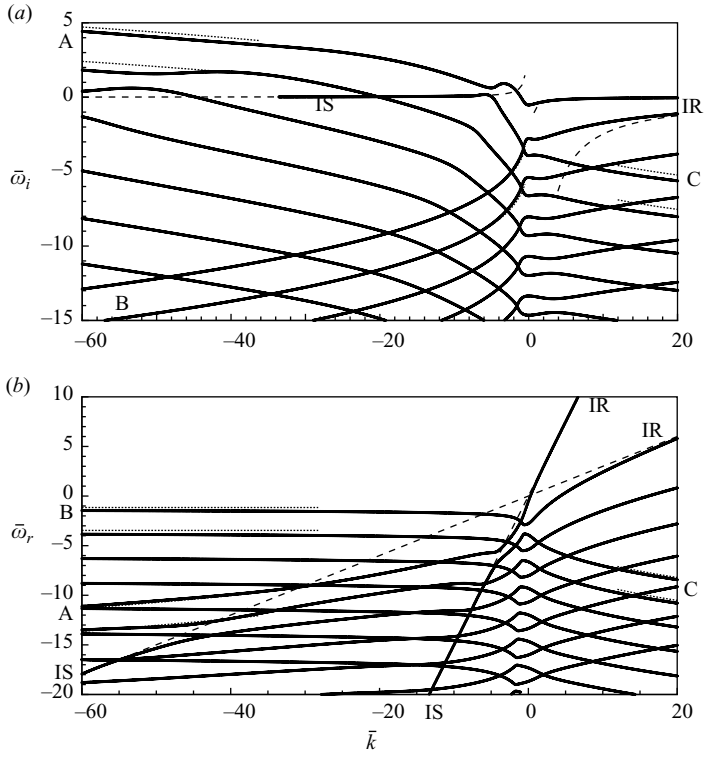

FIGURE 4. Asymptotic results for upper point scalings with $Q = Q_c = 2/9$, $L = 0$ $m = -1$. Details as in figure 2.

As we shall see, in both of these regions, the base-flow parameter Ω_2 does not show up in the analysis; therefore, results obtained with the q-vortex are equivalent to those for the swirling Poiseuille flow. This is also true for more general vortex models provided that Ω_2 is assumed to have the same order of magnitude as Ω_0 (which is a reasonable assumption for a given family of base flows).

6.1. *The 'critical wavenumber' region (region 3)*

We first consider the case where the Reynolds number tends to infinity simultaneously as Ω_0 tends to zero, with the parameter $\check{q}$ defined above being of order one. The relevant scalings in this region are:

$$r = Re^{-1/3}|W_2/2|^{-1/3}\check{r}, \tag{6.2a}$$

$$k = Re^{1/3}|W_2/2|^{1/3}\check{k}, \tag{6.2b}$$

$$\omega = m\Omega_0 + kW_0 + |W_2/2|^{2/3}Re^{-1/3}\check{\omega} + O\left(Re^{-2/3}\right), \tag{6.2c}$$

$$u = \check{u} + O\left(Re^{-1/3}\right), \tag{6.2d}$$

$$v = \check{v} + O\left(Re^{-1/3}\right), \tag{6.2e}$$

$$w = \check{w} + O\left(Re^{-1/3}\right), \tag{6.2f}$$

$$p = |W_2/2|^{1/3}Re^{-2/3}\check{p} + O(Re^{-1}). \tag{6.2g}$$

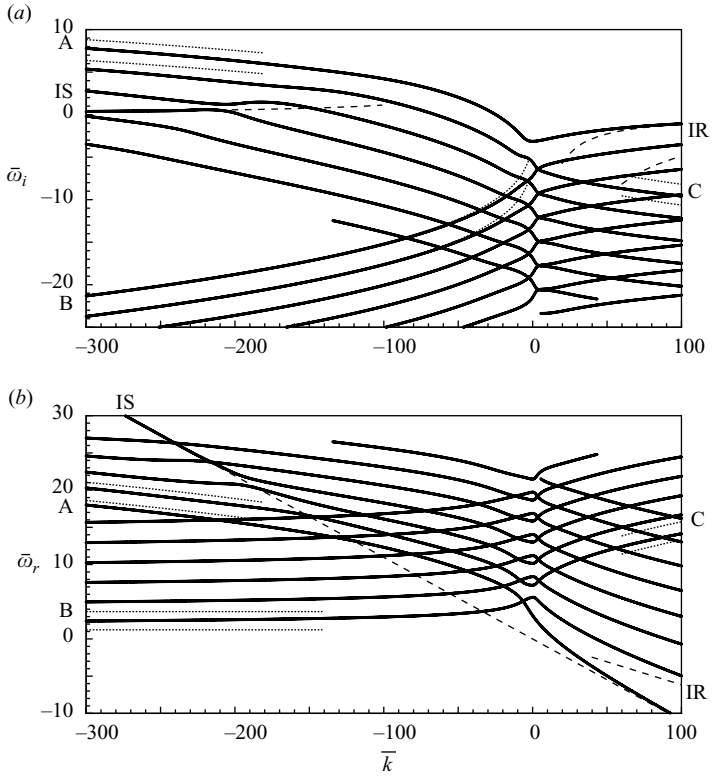

FIGURE 5. Asymptotic results for upper point scalings with $Q = 4$, $L = 0$, $m = -1$. Details as in figure 2.

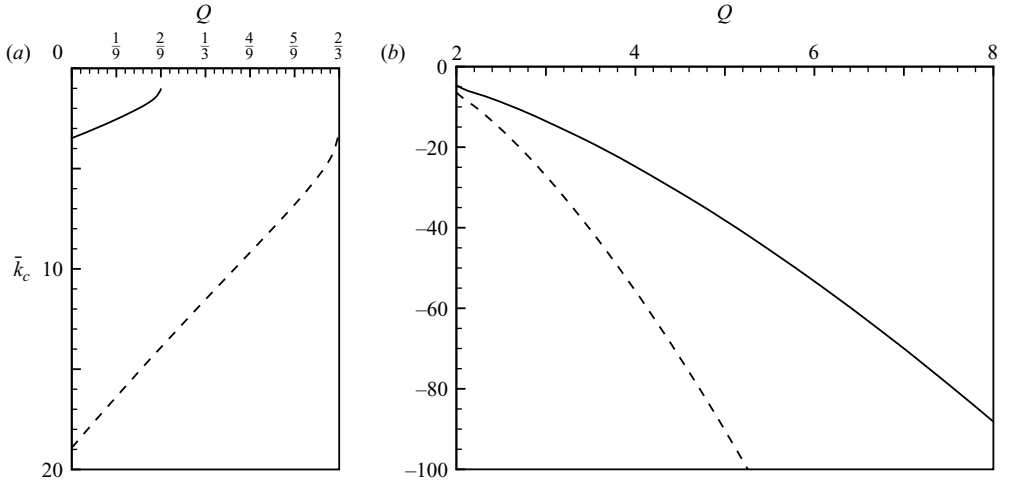

FIGURE 6. Upper point $\bar{k}_c$ as function of Q for $m = -1$ (full line) and $m = -2$ (dashed line) (with $L = 0$). (*a*) Small Q interval ($0 < Q < 2m^2/(m^2 + 8)$). (*b*) Large Q interval ($Q > 2$).

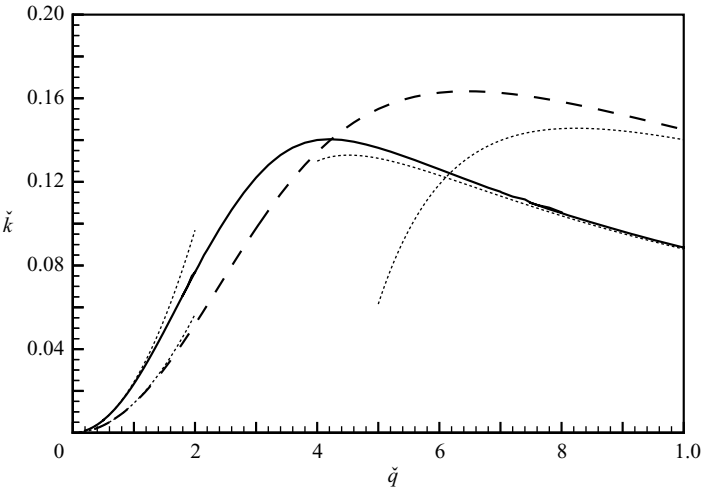

FIGURE 7. Neutral curves in the 'critical wavenumber region' for $m=-1$ (full line) and $m=-2$ (dashed line). The dotted lines indicate the corresponding asymptotic limits for $\check{q} \gg 1$ and $\check{q} \ll 1$.

They permit us to reduce the general eigenvalue problem (2.8) to the following system:

$$-\mathrm{i}(\check{\omega}+\check{k}\check{r}^2)\check{u}-2\check{q}\check{v}+\partial_{\check{r}}\check{p}=\left(\Delta_m-\check{k}^2-\frac{1}{\check{r}^2}\right)\check{u}-\frac{2\mathrm{i}m}{\check{r}^2}\check{v}, \tag{6.3a}$$

$$-\mathrm{i}(\check{\omega}+\check{k}\check{r}^2)\check{v}+2\check{q}\check{u}+\frac{\mathrm{i}m\check{p}}{\check{r}}=\left(\Delta_m-\check{k}^2-\frac{1}{\check{r}^2}\right)\check{v}+\frac{2\mathrm{i}m}{\check{r}^2}\check{u}, \tag{6.3b}$$

$$-\mathrm{i}(\check{\omega}+\check{k}\check{r}^2)\check{w}-2\check{r}\check{u}+\mathrm{i}\check{k}\check{p}=(\Delta_m-\check{k}^2)\check{w}, \tag{6.3c}$$

$$\frac{1}{\check{r}}\frac{\partial}{\partial\check{r}}(\check{r}\check{u})+\frac{\mathrm{i}m}{\check{r}}\check{v}+\mathrm{i}\check{k}\check{w}=0. \tag{6.3d}$$

This system is identical to the full problem in the case where the base flow is a swirling Poiseuille flow with swirl number $\check{q}$ and Reynolds number unity, except that boundary conditions at a finite distance are replaced by vanishing conditions at infinity. Therefore, in this region, all vortex models display similar results and are equivalent to the swirling Poiseuille flow.

The system (6.3) does not seem to be reducible to a single equation for the pressure component as in the other regions. On the other hand, it can easily be reduced to a system of two equations for the u and v components, as was done for example by FJ. Then, it can be solved numerically using the same numerical method as in the other regions, allowing us to compute the eigenfrequencies $\check{\omega}$ as a function of the scaled swirl number $\check{q}$ and the reduced wavenumber $\check{k}$.

Figure 7 shows the marginal stability curves in the $(\check{q},\check{k})$, plane, computed for $m=-1$ and $m=-2$. This curve defines an equation for the upper neutral point which can be termed $\check{k}=\check{k}_{upper}(\check{q})$. The maximum value of this function over all $\check{q}$ is termed $\check{k}_{max}$. The numerical values of $\check{k}_{max}$, as well as the corresponding values of $\check{q}$, are given in table 3. The largest value of $\check{k}_{max}$ is found for $m=-2$.

In the limit $\check{q}\gg 1$, we expect to recover the expression for the 'upper neutral curve' derived in the previous section, i.e. when translated into the current scalings, $\check{k}\approx -m/\check{q}+\bar{k}_{c,0}\check{q}^{-5/2}$. This expression is plotted in figure 7 with dotted lines. The

m	$\check{k}_{max}$	$\check{q}$
-1	0.1404	4.20
-2	0.1634	6.46
-3	0.1583	9.73

TABLE 3. Numerical values for the 'critical wavenumber' $\check{k}_{max}$ and the corresponding parameter $\check{q}$.

asymptotic expression for $\check{q} \ll 1$, to be derived in § 6.2, is also plotted in a similar way. Both these limits are correctly recovered.

6.2. *The 'left neutral curve' region*

This last region corresponds to the case of very small swirl numbers. This region was analysed in § 4 of SNB in the case of the swirling Poiseuille flow. SNB referred to this case as the 'lower neutral curve' in a Reynolds number/swirl number diagram. Here, as all results are interpreted in terms of the (q, k) diagram, we find it more appropriate to refer to this case as the 'left neutral curve' region (see figure 1).

This region can be investigated by letting both q tend to zero and Re tend to infinity in the starting equations with k remaining of order one, as was initially done by SNB. However, it is just as simple to start from the system of the previous section and let $\check{k}$ tend to zero with $\check{q} \approx \check{k}^{1/2}$. To recover the expressions of SNB, we introduce the following notation:

$$\left.\begin{aligned} &\check{q} = (-m)\check{k}^{1/2}\sigma, \quad \check{\omega} = \check{k}^{1/2}\lambda, \quad \check{r} = \check{k}^{-1/4}s, \\ &\check{u} = \mathrm{i}\bar{g}_1, \quad \check{v} = \bar{h}_1, \quad \check{w} = \check{k}^{-3/4}\bar{f}_1, \quad \check{p} = \check{k}^{1/4}\bar{p}_1. \end{aligned}\right\} \tag{6.4}$$

Note that in terms of the primitive parameters, the parameter σ (which is actually a rescaled swirl number) and the scaled frequency λ are defined as follows:

$$\sigma = \Omega_0 |W_2/2|^{-1/2} k^{-1/2} (-m)^{-1} Re^{1/2}, \tag{6.5}$$

$$\omega = kW_0 + m\Omega_0 + |W_2/2|^{1/2} k^{1/2} Re^{-1/2}\lambda. \tag{6.6}$$

Introducing this notation into (6.3) and letting $\check{k}$ tend to zero leads directly to system (4.5) of SNB, which is reproduced below:

$$(\lambda + s^2)\bar{g}_1 + 2m\sigma\bar{h}_1 + \partial_s\bar{p}_1 = \mathrm{i}\left(\Delta_m - \frac{1}{s^2}\right)\bar{g}_1 - \frac{2\mathrm{i}m}{s^2}\bar{h}_1, \tag{6.7a}$$

$$(\lambda + s^2)\bar{h}_1 + 2m\sigma\bar{g}_1 - \frac{m\bar{p}_1}{s} = \mathrm{i}\left(\Delta_m - \frac{1}{s^2}\right)\bar{h}_1 + \frac{2\mathrm{i}m}{s^2}\bar{g}_1, \tag{6.7b}$$

$$(\lambda + s^2)\bar{f}_1 - 2s\bar{g}_1 = \mathrm{i}\Delta_m\bar{f}_1, \tag{6.7c}$$

$$\frac{1}{s}\frac{\partial}{\partial s}(s\bar{g}_1) + \frac{m}{s}\bar{h}_1 + \bar{f}_1 = 0. \tag{6.7d}$$

This eigenvalue problem was solved by SNB, and the solutions λ as function of σ are shown in their figures 10 and 11 for $m = -1$ and -2. For the sake of completeness, we reproduce the result for $m = -1$, obtained using the present numerical method, in our figure 8. This plot displays the same general trends as observed in the other regions of the neutral curves. On the 'stable' side $\sigma < 0$, we recognize two series of branches which display either the inviscid behaviour or the viscous C behaviour. On

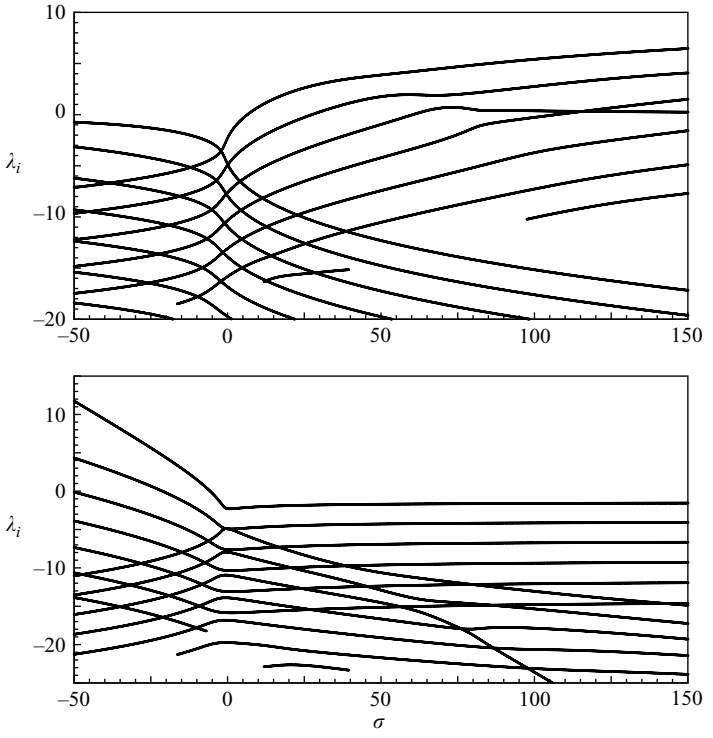

FIGURE 8. Asymptotic results in the 'left neutral curve' region (case $m=-1$).

m	σ_c	λ
−1	6.425	−5.841
−2	4.202	−7.592
−3	4.152	−9.520

TABLE 4. Values of the 'left' neutral point σ_c and the corresponding frequency λ for $m=-1,-2,-3$.

the 'unstable' side $\sigma>0$, we recognize branches with the viscous A and B behaviour as well as one branch with the inviscid singular behaviour.

Finally, the location of the neutral curve is defined by the value σ_c where the first branch becomes unstable. The numerical values of σ_c for $m=-1,-2,-3$ as well as the corresponding frequencies are given in table 4. The results for $m=-1$ are in accordance with the value $\sigma_c\approx 6.45$ given in SNB.

Coming back to the primitive parameters, we can note that the location of the left neutral curve is given, whatever the precise base flow, by

$$\Omega_0|W_2/2|^{-1/2}k^{-1/2}(-m)^{-1}Re^{1/2}=\sigma_c. \tag{6.8}$$

Note that when expressed in the variables of the previous section, this condition takes the much simpler form:

$$\check{k}=\left(\frac{\check{q}}{m\sigma_c}\right)^2. \tag{6.9}$$

This expression is plotted in figure 7, and gives, as expected, the limit for $\check{k} \ll 1$ of the neutral curve.

7. Application to the q-vortex

In this section, we apply our asymptotic results to the q-vortex, and compare with numerical results directly taken from FJ or obtained with the same numerical method.

7.1. *The neutral curves*

We first gather the results obtained in the previous sections for the location of the neutral curves.

For the lower neutral curve region:

$$k_{lower} = Re^{-1/2} q^{1/2} \underline{k}_c, \tag{7.1}$$

with $\underline{k}_c$ given in table 1.

For the critical swirl region:

$$Re^{1/2} q^{-1/2} k \left[1 + \frac{qk}{m}\right] = \underline{k}_c. \tag{7.2}$$

For the upper neutral curve region (outside of the forbidden interval):

$$k_{upper} = -m/q + Re^{-1/2} q^{-5/2} \bar{k}_c, \tag{7.3}$$

where $\bar{k}_c$ depends upon the swirl number q and is given in figure 6 with $Q = q^2$.

For the critical wavenumber region:

$$k = Re^{1/3} \check{k}_{upper}(\check{q}), \tag{7.4}$$

where $\check{q} = Re^{1/3} q$, and the function $\check{k}_{upper}(\check{q})$ is defined by figure 7.

For the left neutral curve region:

$$q_{left} = |m| k^{1/2} Re^{-1/2} \sigma_c, \tag{7.5}$$

where σ_c is given in table 4.

Figure 9 shows the neutral curves in the case $Re = 10^4$, $m = -1$. The thick lines correspond to the numerical results. The thin dotted dashed and dash-dotted lines correspond, respectively, to the approximations (7.2), (7.3) and (7.4). The very thin line shows the leading-order approximation of the 'upper neutral curve', i.e. $k = -m/q$. The approximations (7.1) and (7.5) are not shown since they constitute particular cases of (7.2) and (7.4).

As can be observed, the agreement with the asymptotic prediction is good for the lower and upper neutral curves. The agreement is less good in the critical swirl number and critical wavenumber regions. This is not surprising since the asymptotic analyses in these regions require, respectively, $q \gg 1$ and $k \gg 1$, which are far from being verified here. The left neutral curve is in good agreement with the asymptotics for $k \approx 2$. Note that the numerically obtained neutral curve departs from the asymptotic prediction for $k < 1.4$ and extends into the region of negative swirls. This is due to the existence of inviscid instabilities in this region (Mayer & Powell 1992). This part of the neutral curve is not shown in the figure. The location of the 'forbidden interval' of the 'upper neutral curve' is also indicated. As can be observed, in this interval, the 'upper neutral curve' is given by its leading order, $k = -m/q$, with an excellent approximation.

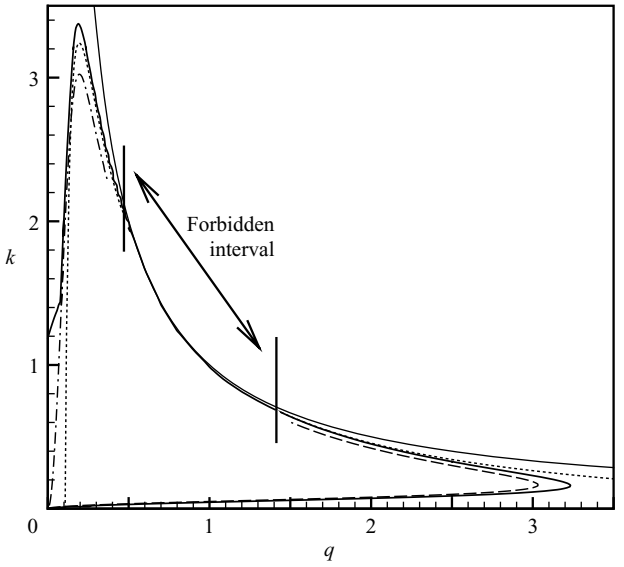

FIGURE 9. Neutral curves in the (k, q)-plane for the q-vortex, for $Re = 10^4$ and $m = -1$. Full line, numerical result from Fabre & Jacquin (2004). Dashed lines, equation (7.2). Dotted line, equation (7.3). Dash-dotted line, equation (7.4). Thin line, $k = -m/q$.

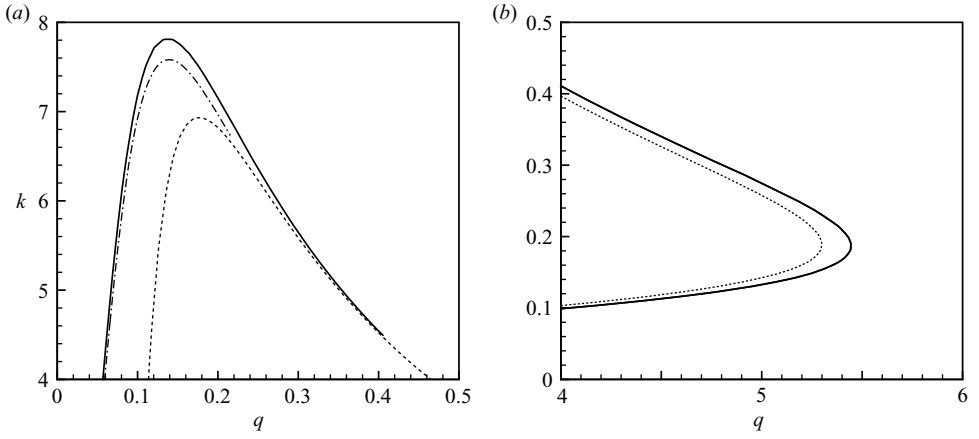

FIGURE 10. As in figure 9 but for $m = -2$ and $Re = 10^5$. (a) Critical wavenumber region; (b) critical swirl number region.

A second comparison case, which corresponds to $m = -2$, $Re = 10^5$, is shown in figure 10. Only the critical swirl and critical wavenumber regions are depicted. Here, a reasonable agreement with the asymptotic predictions is observed in both regions.

7.2. *Temporal branches*

We now consider the temporal branches (i.e. ω as function of k) described in § 4.1 of FJ and compare with the various asymptotic predictions. We consider only one case, corresponding to $q = 2, m = -1, Re = 5 \times 10^5$. Figure 11($a$) displays the amplification rate ω_i, and figure 11(b) displays the relative oscillation rate $\omega_r - (mq + k)$ (i.e. relative to the frame of the vortex centre). The thick grey lines correspond to the numerical

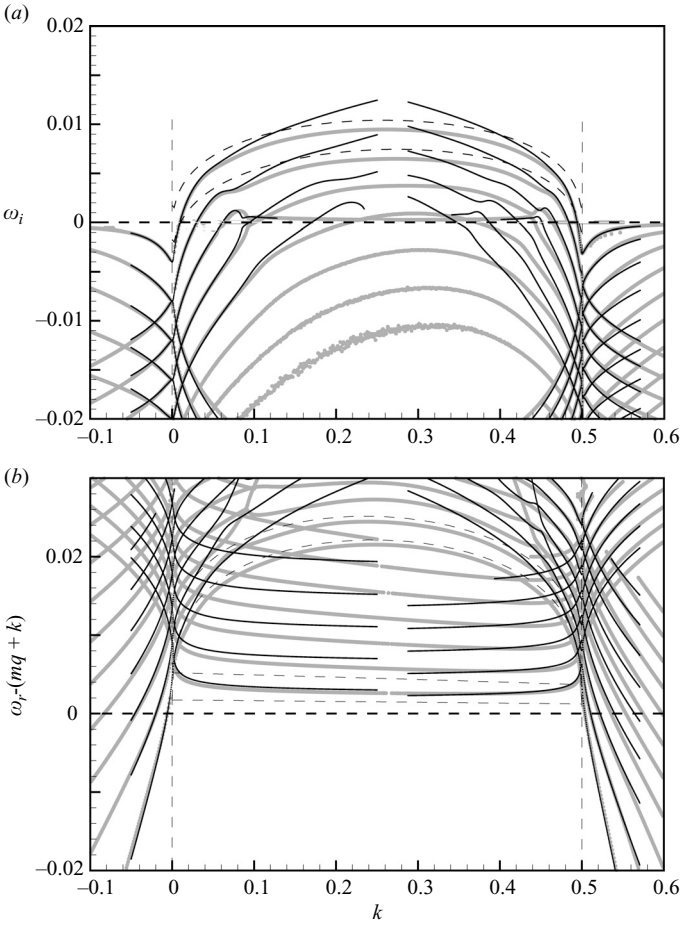

FIGURE 11. Amplification rate ω_i and relative oscillation rate $\omega_r - (mk + q)$ for the q-vortex with $m = -1$, $q = 2$, $Re = 5 \times 10^5$. Thick grey lines: numerical results from Fabre & Jacquin (2004). Thin black lines: asymptotic results for lower neutral curve and upper neutral curve scalings. Dashed lines: Asymptotic result for modes A and B of Le Dizès & Fabre (2007).

results taken from figure 5(f) of FJ. The thin lines correspond to the asymptotic results with the lower and the upper neutral curves scalings (from figures 2 and 5 of the present paper). Finally, the dashed lines give the asymptotic prediction from LDF for the two first viscous modes of kinds A and B.

The figures nicely illustrate how the different approximations match together. For $k < 0.1$ and $k > 0.4$, the numerical results closely follow the results with the neutral curve scalings. On the other hand, in the central region of the plots, the predictions of LDF apply, and give a good estimation to the numerical branches. The agreement with the latter estimate is less good than in the neutral curve regions, but it must be remembered that the analysis of LDF requires $Re^{-1/6} \ll 1$ versus $Re^{-1/4} \ll 1$ for the present analyses.

As a final remark, the branch which displays the 'inviscid singular' behaviour in both neutral curve regions actually extend throughout the whole range of k. This branch will be considered specifically in § 7.4.

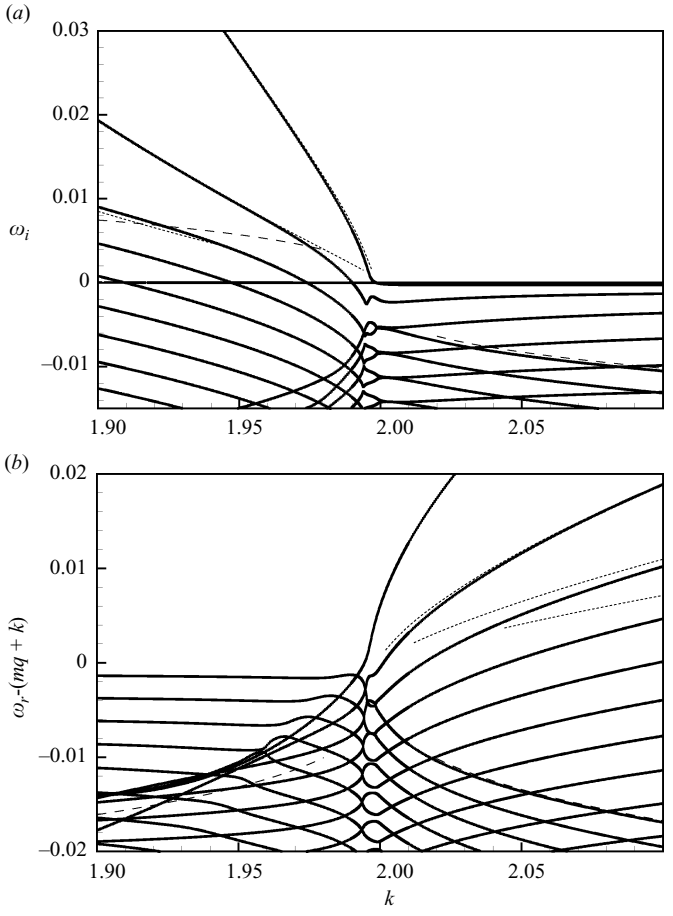

FIGURE 12. Results for the q-vortex in the vicinity of the 'upper neutral curve' for $q=1$, $m=-2$ (in the forbidden interval). Full lines, numerical results for $Re=10^6$. Dashed lines, predictions for viscous modes A and B. Dotted lines, numerical results in the inviscid case.

7.3. *The 'forbidden interval'*

Finally, we have mentioned in § 5.1 that centre modes are not expected to be found in the vicinity of the 'upper neutral curve' for values of q lying in a 'forbidden interval'. To illustrate this case we present (figure 12) the numerical result obtained in the vicinity of $k=-m/q$ for the case $m=-2$, $q=1$, which falls within this interval. The full lines correspond to numerical results for $Re=10^6$. The dotted lines correspond to numerically obtained inviscid results. The dashed lines correspond to the asymptotic prediction of LDF for the first modes of types A and C.

As can be observed, the C mode is approached by a numerical branch on the stable side. On the other hand, the A mode does not seem to be approached. Instead, we observe several unstable branches whose frequencies are predicted well by the inviscid results. These branches correspond to the well-known inviscid instabilities existing in this region of parameters (see e.g. Leibovich & Stewartson 1983; Mayer & Powell 1992). The structure of these latter instabilities near the 'upper neutral curve' $k\approx -m/q$ was investigated by Stewartson & Capell (1985) who demonstrated that

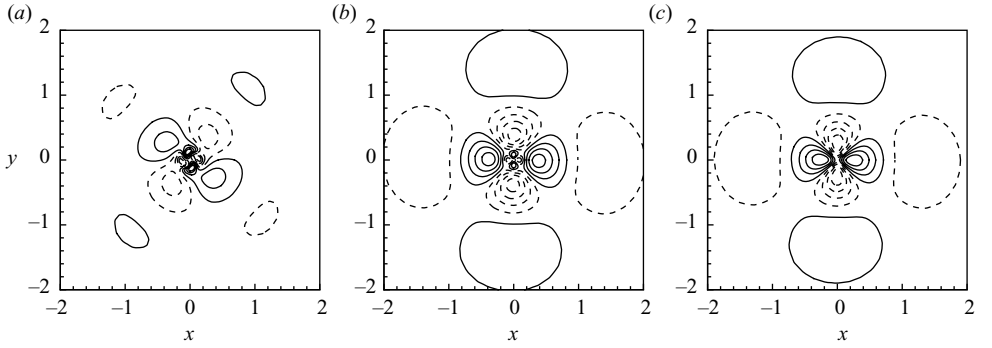

FIGURE 13. Structure of some eigenmodes computed for $q = 1$, $m = -2$, $Re = 10^6$. Iso-contours of the axial velocity component; eight equally spaced levels with dashed negative. (*a*) Most amplified mode for $k = 1.95$; (*b*) neutral mode for $k = 1.99838$; (*c*) less damped mode for $k = 2.05$.

for large $|m|$ they become ring modes, with therefore a completely different nature than the centre modes considered here.

Figure 13 shows the shapes of three modes computed on the most unstable branch, for $k = 1.95$, $k = 1.99838$ (which corresponds to the point where this branch becomes neutral) and $k = 2.05$. It can be observed that, even though some of them display strong gradients at the vortex centre, none of these modes is strictly of centre mode type; instead they all extend to the whole vortex core region. This confirms our expectations that centre modes do not exist in this region of the 'upper neutral curve'.

7.4. *The inviscid near-neutral modes existing inside the unstable domain*

In §§ 3.2.2 and 5.2.2 (and in Appendices B and C) it has been shown that on the unstable side of the lower and upper neutral curves, there exist some modes which are solutions of the inviscid equations but are singular at a critical point located along the real r-axis. It was subsequently verified that these modes are effectively attained as a limit of branches computed from the viscous equations, and that viscosity has a destabilizing effect on them. In this section, we adress the significance of these modes in the strictly inviscid case and their relations with centre modes evidenced in other inviscid studies.

For the case of the q-vortex, the existence of inviscid centre modes in the regions considered here was investigated using asymptotic techniques by Stewartson & Brown (1985). Their analysis is similar to that reproduced in our Appendices B and C, except that instead of requiring the solutions to vanish away from the central region, they imposed a matching condition with an outer solution. Their study focused mainly on the vicinity of the 'upper neutral curve'. The main result is their equation (4.15), which can be set in the following form:

$$\omega = (mq + k) - q^2 C_1 \kappa + \frac{A}{B} \exp(-\mathrm{i}\alpha_1 \pi) C_2 \kappa^{\alpha_1 + 1}, \tag{7.6}$$

where $\kappa = -(k + m/q)$ is the distance from the neutral curve, C_1 is identical to that defined in our equation (C 11), C_2 is a positive term depending upon q, m and the index n of the family, A/B is a constant arising from the matching with the outer solution and α_1 is the same as defined in (5.9), and amounts to $\alpha_1 = \sqrt{m^2 + 8q^2/(q^2 - 2)}$ for the q-vortex.

It can be observed that the two first terms in this expression are identical to those obtained in our case. Moreover, the additional term may have a positive or negative imaginary part, depending upon the sign of $(A/B)\sin\alpha_1\pi$. When this quantity is negative, this expression predicts unstable modes. In this case, the critical point r_c acquires a small positive imaginary part, and the corresponding mode becomes regular for all real values of r. Stewartson & Brown (1985) showed that this situation occurs in several intervals of q, the largest of all being found for $|m|=1$ and extending up to $q=2.31$. This prediction was confirmed numerically by Heaton (2007).

When the quantity $(A/B)\sin\alpha_1\pi$ is positive, (7.6) predicts damped modes. In this case, the critical point r_c acquires a small negative imaginary part, and the structure of the corresponding eigenmode is singular along a branch cut originating from the critical point and intersecting the real axis. This case was excluded by Stewartson & Brown (1985) who concluded that in such a case there are no inviscid centre modes in this region. However, such singular damped modes may still be significant in a viscous context and provide the leading order of modes computed from the viscous equations. Note that modes with such a peculiar structure are not uncommon in vortex flows: they were found, for example, in the two-dimensional problem by Briggs, Daugherty & Levy (1970), and in the three-dimensional stability of the Lamb–Oseen vortex by Fabre *et al.* (2006).

According to this discussion it is clear that the modes investigated in Stewartson & Brown (1985) and in the present study all belong to the same family, as their frequencies are identical at leading order. We now wonder, of the viscous correction computed in the present work and the inviscid one computed by Stewartson & Brown (1985), which is the most significant. Let us consider, for example, the case $q=2, m=-1$, $k=0.45$ (i.e. $\kappa=0.05$) and the first mode of the family (with index $n=0$). In that case, (7.6) applies with $\alpha_1=\sqrt{17}$, $C_2=3.025$, $A/B\sin\alpha_0\pi\approx-0.06$, and leads to $\omega_i\approx 0.18\kappa^{1+\sqrt{17}}\approx 4\times10^{-8}$, in agreement with the order of magnitude of the numerical result of Heaton (2007). Our own study predicts $\omega_i=-(D_1/8)Re^{-1}\kappa^{-1}$ with $D_1=-113.26$. Comparing both expressions, it is found that the condition for the viscous correction to be larger than the inviscid one is $Re\leqslant 7\times10^{10}$. Similar arguments can be invoked in the vicinity of the lower neutral curve. This case was investigated briefly by Stewartson & Brown (1985) who concluded that inviscid unstable modes do not exist in this case. However, their results also allow the existence of singular damped modes in this case. Reiterating their analysis leads to the inviscid prediction $\omega_i\approx-64\pi/729q^{-4}k^4$. In situations of practical interest (i.e. $q>1.5, Re<10^9$) this expression always remains several orders of magnitudes smaller than the viscous prediction obtained from (3.11), which corresponds in this case to $\omega_i\approx DqRe^{-1}k^{-1}$ with $D=96/7$.

Therefore, it can be concluded that under circumstances of practical interest, the inviscid prediction of Stewartson & Brown (1985) will be several orders of magnitude smaller than the viscous correction computed herein, and that the modes will be unstable owing to viscous effects, whatever the precise details of the singularity structure of the inviscid solution. Moreover, these modes will always remain much less amplified compared to the viscous modes existing in the same region.

8. Long-wave centre modes in pure vortices

In § 3, we have described the centre modes existing in the long-wave range assuming that $W_2\neq0$. Here, we consider the case $W_2=0$, which corresponds to a 'pure' vortex

without axial flow. It turns out that, although the scalings are slightly different, the results in this case can actually be deduced directly from those of § 3. We briefly present the asymptotic derivation and apply the results to the Lamb–Oseen vortex.

8.1. *Asymptotic scalings*

In this case, the scalings that allow us to reduce the equations to the most generic form are:

$$r = Re^{-1/4}|\Omega_2|^{-1/4}\tilde{r}, \tag{8.1a}$$

$$k = Re^{-1/4}|\Omega_2|^{3/4}|\Omega_0|^{-1}\tilde{k}, \tag{8.1b}$$

$$\omega = m\Omega_0 + Re^{-1/2}|\Omega_2|^{1/2}\tilde{\omega} + O(Re^{-1}), \tag{8.1c}$$

$$u = \tilde{u} + O\left(Re^{-1/2}\right), \tag{8.1d}$$

$$v = \tilde{v} + O\left(Re^{-1/2}\right), \tag{8.1e}$$

$$w = \tilde{w} + O\left(Re^{-1/4}\right), \tag{8.1f}$$

$$p = Re^{-1/4}\Omega_0|\Omega_2|^{-1/4}\tilde{p} + O\left(Re^{-3/4}\right), \tag{8.1g}$$

$$\xi_z = Re^{1/4}|\Omega_2|^{1/4}\tilde{\xi} + O\left(Re^{-1/4}\right). \tag{8.1h}$$

Note that the scalings for ω and r are actually the same as in § 3.1, but the scaling for k is different.

Repeating the analysis of § 3.1 with these scalings, we see that at leading order, the radial and azimuthal momentum equations still lead to the geostrophic balance (3.3) and that the vorticity equation still leads to the same equation as (3.7), i.e.:

$$-\mathrm{i}\left(\frac{1}{2}m\tilde{r}^2 + \tilde{\omega}\right)\Delta_m\tilde{p} = -4\mathrm{i}m\tilde{p} + 4\mathrm{i}\tilde{k}\tilde{w} + \Delta_m^2\tilde{p}. \tag{8.2}$$

On the other hand, the axial momentum equation now takes the form

$$-\mathrm{i}\left(\frac{1}{2}m\tilde{r}^2 + \tilde{\omega}\right)\tilde{w} = -\mathrm{i}\tilde{k}\tilde{p} + \Delta_m\tilde{w}. \tag{8.3}$$

These two equations can be combined into the following sixth-order differential equation:

$$\mathrm{i}\left(\frac{1}{2}m\tilde{r}^2 + \mathrm{i}\tilde{\omega} + \Delta_m\right)\left[\mathrm{i}\left(\frac{1}{2}m\tilde{r}^2 + \mathrm{i}\tilde{\omega} + \Delta_m\right)\Delta_m - 4\mathrm{i}m\right]\tilde{p} = -4\tilde{k}^2\tilde{p}. \tag{8.4}$$

It turns out that this equation is identical to (3.8) with the following substitution:

$$m\underline{k} \equiv \tilde{k}^2. \tag{8.5}$$

Therefore, the results in the present case can be deduced directly from those obtained in § 3. For $m < 0$, the results obtained for $\underline{k} < 0$ are relevant, and have to be applied for both signs of $\tilde{k}$. This means, in particular, that all modes are stable. For $m > 0$, results can be deduced from the symmetry $(m, \omega) \leftrightarrow (-m, -\omega^*)$, leading again to stable modes only.

We can also use the results of § 3.2 to predict the limits for large $\tilde{k}$. The two possible limits are the inviscid regular modes and the viscous modes of type C. For the inviscid modes, we expect

$$\tilde{\omega} \equiv \frac{C(m,n)}{m}\tilde{k}^2 + \mathrm{i}\frac{mD(m,n)}{\tilde{k}^2}, \tag{8.6}$$

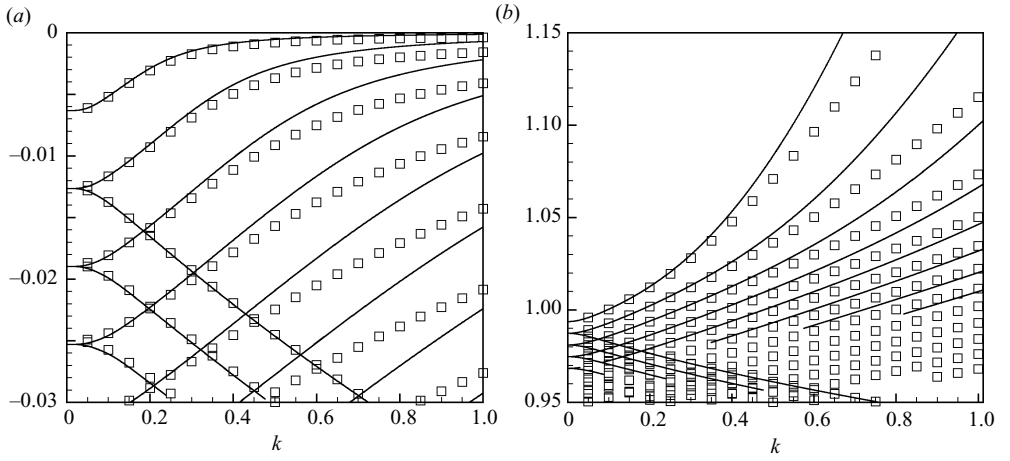

FIGURE 14. Frequencies of the long-wave centre modes of the Lamb–Oseen vortex (*a*) imaginary part; (*b*) real part. Symbols; numerical results for $m=1$, $Re=10^5$. Thin lines, asymptotic results.

or, equivalently, in terms of the primitive variables,

$$\omega \approx m\Omega_0 + \frac{C(m,n)}{-\Omega_2 m}k^2 + \mathrm{i}\frac{m\Omega_2^2 D(m,n)}{Rek^2}. \tag{8.7}$$

Note that, because of the symmetry $D(m,n)=-D(-m,n)$, the last part of these expressions predicts damping for both $m>0$ and $m<0$. For the viscous C modes, we have the following behaviour for $m>0$:

$$\tilde{\omega} \approx 3|m|^{4/3}|\tilde{k}|^{2/3}\mathrm{e}^{-\mathrm{i}\pi/6} + (n+1/2)\sqrt{6|m|}\mathrm{e}^{-\mathrm{i}\pi/4} \qquad (n=0,1,2,\ldots), \tag{8.8}$$

while for $m<0$ the real part of $\tilde{\omega}$ is reversed.

8.2. *Application to the Lamb–Oseen vortex*

To illustrate these results, we consider the case of the Lamb–Oseen vortex, as defined by (2.6). A comprehensive analysis of the normal modes of this vortex was given in Fabre *et al.* (2006). They observed that two families of modes, which they called modes C and V, acquire a centre mode behaviour in the long-wavelength limit. These two families correspond, respectively, to the 'inviscid regular' and 'viscous C' modes of the present nomenclature.

Numerical and asymptotic results are compared for a single case, corresponding to $Re=10^5$ and $m=1$. The damping rates ω_i and the frequencies ω_r are displayed, respectively, in figures 14(*a*) and 14(*b*). The symbols are full numerical results, and the thin lines are asymptotic results deduced from those plotted in the stable side (i.e. $\bar{k}<0$) of figure 2. A close agreement between the numerics and the asymptotic predictions is observed up to $k\leqslant 0.3$.

9. Summary

The primary objective of this paper was to obtain the marginal stability curves for the family of viscous centre modes in vortices evidenced in FJ and LDF. The study was conducted for the general case of a vortex described by the Taylor coefficients Ω_0, Ω_2, W_0, W_2, etc... of the rotation rate and axial velocity at the vortex centre.

For the purpose of the study, we have been lead to consider successively five regions of the neutral curve. In each region, we have reduced the stability to a generic system which was numerically solved. In all regions but one, the results are universal and apply to all possible vortex models. In particular, the results of SNB, initially derived in the case of the swirling Poiseuille flow, are recovered as particular cases of our study. The most complicated region turned out to be the vicinity of the 'upper neutral curve'. In this region results are not universal but depend upon two base-flow parameters Q and L. Moreover, we showed that there is an interval of this 'upper neutral curve' where marginal modes are not centre modes but have a more complicated structure.

In practice, the most important result was obtained when considering the critical swirl region. The study of this region allowed us to obtain a necessary and sufficient condition for the occurrence of unstable centre-modes:

$$|\Omega_2||W_2/2|^{-4/3} < 0.1408Re^{1/3}. \tag{9.1}$$

This condition is more precise than that given by LDF, who were able to show that a vortex is unstable in the large-Reynolds-number limit whenever $\Omega_0 W_2 \neq 0$.

In addition to the mapping of the neutral curves, we have investigated the relations between the viscous unstable centre modes and other kinds of centre modes. We have found that in the vicinity of each neutral curve, four other families are always present. Two of them are stable and of viscous nature, and were described by LDF. The third family corresponds to inviscid regular modes, which are weakly damped by viscosity, and are found on the 'stable' side of the neutral curves. The last family are called 'inviscid singular' modes because their structure is, at leading order, a solution of the inviscid equation, except in the vicinity of a critical point located along the real r-axis. These modes are unstable and exist in the same regions as the unstable viscous centre modes, but are always much less amplified. In the strictly inviscid case, and for the case of the q-vortex, these modes are of the same nature as those previously investigated by Stewartson & Brown (1985) and Heaton (2007), which may be regular and unstable or singular and damped. However, we have shown that under situations of practical interest, the amplification rate of these modes is determined by viscous effects whatever the exact details of their inviscid structure.

In each of the regions studied, a complex reorganization between the various families of centre modes occurs. The various kind of branches exchange their identities, from viscous to inviscid, from unstable to stable and vice versa. All possible situations seem to occur, depending on the region considered. Such a behaviour was evidenced for the swirling Poiseuille flow by SNB. Our systematic study showed the universality and the complexity of this behaviour.

This work has been supported by the European Community under grant AST4-CT-2005-012238 (FAR-WAKE project) and by the French National Research Agency (Vortex project).

Appendix A. The two-dimensional centre modes

In this Appendix, we describe the centre modes existing in the two-dimensional case, obtained by imposing $k = 0$ in either of the analyses of §§ 3 and 8. We consider, for simplicity, the case of a 'pure vortex' and set $\tilde{k} = 0$ in (8.2) and (8.3). This leads to

two decoupled equations with the following forms:

$$-\mathrm{i}\left(\tfrac{1}{2}m\tilde{r}^2+\tilde{\omega}\right)\tilde{w}=\Delta_m\tilde{w}, \tag{A 1}$$

$$-\mathrm{i}\left(\tfrac{1}{2}m\tilde{r}^2+\tilde{\omega}\right)\Delta_m\tilde{p}=-4\mathrm{i}m\tilde{p}+\Delta_m^2\tilde{p}. \tag{A 2}$$

Therefore, in the two-dimensional case, we have two distinct kinds of eigenmodes, which we call the w-modes and the p-modes, respectively. Note that in a strictly two-dimensional framework where an axial velocity is not allowed, only the p-modes are relevant.

Equation (A 1) governing the w-modes is recognized as an equivalent of the parabolic cylinder equation in cylindrical coordinates. The general solution of this equation can be written as follows:

$$\tilde{w}=s^{|m|}\exp(-s^2)M(a;b;2s^2), \tag{A 3}$$

where M denotes the confluent hypergeometric function, also called Kummer's function (Abramowitz & Stegun 1965), and where the terms entering the expression are defined as follows:

$$s=\sqrt{\frac{-\mathrm{i}m}{8}}\tilde{r},\quad a=\frac{|m|+1}{2}-\frac{\tilde{\omega}}{\sqrt{2\mathrm{i}m}},\quad b=|m|+1. \tag{A 4}$$

In the expression (A 3), the Kummer function is generally an exponentially growing function, and the expression does not lead to an eigenmode solution vanishing at $\tilde{r}\to\infty$. However, when a is zero or a negative integer, say $a=-n$, the Kummer function reduces to a polynomial, thus leading to a bounded solution. This condition gives the general expression for the frequencies of the w two-dimensional modes:

$$\tilde{\omega}=\sqrt{2\mathrm{i}m}(1+|m|+2n)\qquad(N=0,1,2,\ldots). \tag{A 5}$$

Equation (A 2) governing the p-modes is a fourth-order equation related to the parabolic cylinder equation. We did not succeed in giving a general solution of this equation in analytic form. However, the numerical solution strongly suggests that the frequencies of the p modes are actually given by:

$$\tilde{\omega}=\sqrt{2\mathrm{i}m}(\sqrt{m^2+8}+1+2n). \tag{A 6}$$

We have verified numerically the validity of this expression for $m=1,2,3$ and n up to 20 and found excellent agreement (up to at least 5 decimal places using 150 collocation points).

Note that Bajer, Bassom & Gilbert (2001) have derived and studied the time-dependent version of (A 2) (with the frequency $\tilde{\omega}$ replaced by a time derivative). They were able to give a time-dependent solution to this equation in closed form. The large-time behaviour of their solution is exponential, and corresponds to the first frequency predicted by (A 6) (with $n=0$). They also gave the expression of the corresponding eigenmode:

$$\tilde{p}=s^{|m|}M\left(\frac{\sqrt{m^2+8}+|m|}{2},|m|+1,-s^2\right). \tag{A 7}$$

Despite repeated efforts, we have not been able to generalize this expression for the higher-order eigenmodes.

It can be observed that a degeneracy occurs for $|m|=1$: the p-mode number n has the same frequency as the w-mode number $n+1$. So, the eigenmodes are expected to come in pairs with the same frequency, except for the first w-mode (with $n=0$) which is alone. This degeneracy does not occur for $|m|>1$ where the frequencies of the p and w modes are always distinct.

In the case $W_2 \neq 0$ considered in § 3, the scaling for the frequency is the same, so the formulae (A 5) and (A 6) can be used to predict $\underline{\omega}$. However, the equations obtained for $k=0$ are not completely decoupled because the equation for w also contains a term involving p. Therefore, the p-modes also have a w component.

Appendix B. The inviscid centre modes in the long-wave range

Here, we describe the centre modes solutions existing in the long-wave range that are inviscid at leading order. As explained in § 3.2.2, such modes can be described by either letting the Reynolds number tend to infinity in the primitive equations (with fixed k), expanding the solution in powers of Re^{-1}, and then letting $k \to 0$, or by letting $\underline{k} \to \infty$ in the equations obtained with the scalings of § 3. We chose the second way which allows us to start directly from the equations of § 3. Therefore, we consider the following expansions for the frequency and the eigenmode:

$$\underline{\omega} = C\underline{k} + \frac{\mathrm{i}D}{\underline{k}} + O(\underline{k}^{-3}), \tag{B 1}$$

$$\underline{p} = \underline{p}^{(0)} + \underline{k}^{-2}\underline{p}^{(1)}. \tag{B 2}$$

Then, we substitute this expansion into (3.8). At leading order, we obtain:

$$\left(\tfrac{1}{2}m\underline{r}^2 + C\underline{k}\right)^2 \Delta_m \underline{p}^{(0)} - 4m\left(\tfrac{1}{2}m\underline{r}^2 + \underline{k}\right)\underline{p}^{(0)} + 4\underline{k}m\,\underline{p}^{(0)} = 0. \tag{B 3}$$

It is then convenient to introduce a new variable s, defined in terms of $\underline{r}$ (and in terms of the primitive variable r) as follows:

$$s^2 = \frac{m\underline{r}^2}{2C\underline{k}} \qquad \left[= \frac{2\Omega_2^2}{-W_2\Omega_0}\frac{mr^2}{2Ck}\right]. \tag{B 4}$$

With this ansatz, (B 3) is the following compact form:

$$(s^2+1)^2\Delta_m \underline{p}^{(0)} - 8\left(s^2 + 1 - \frac{1}{C}\right)\underline{p}^{(0)} = 0, \tag{B 5}$$

where the notation Δ_m is now the two-dimensional Laplacian operator operating on the variable s. This equation admits a solution in terms of the hypergeometric function F (Abramowitz & Stegun, 1965), with the following form:

$$\underline{p}^{(0)} = s^{|m|}(1+s^2)^{-\mu}F(a,b;|m|+1;-s^2); \tag{B 6}$$

$$\mu(\mu+1) = \frac{2}{C}, \tag{B 7}$$

$$a = -\mu + \frac{|m|-\alpha_0}{2}, \tag{B 8}$$

$$b = -\mu + \frac{|m|+\alpha_0}{2}, \tag{B 9}$$

with, again,

$$\alpha_0 = \sqrt{m^2+8}. \tag{B 10}$$

This expression does not, in general, describe an eigenfunction vanishing at $s \to \infty$. The exception is met when b is zero or a negative integer, say $b = -n$. This condition gives the allowed values for the group velocity coefficient $C(m, n)$:

$$C(m,n) = \frac{8}{(|m| + \sqrt{m^2+8} + 2n)(|m| + \sqrt{m^2+8} + 2n + 2)}. \tag{B 11}$$

Furthermore, in such cases, the hypergeometric function reduces to a polynomial. For example, we detail the structure of the eigenmodes corresponding to the three lowest values of n:

$$\underline{p}^{(0)} = \frac{s^{|m|}}{(1+s^2)^{(|m|/2+\alpha_0/2)}} \quad (n=0), \tag{B 12a}$$

$$\underline{p}^{(0)} = \frac{s^{|m|}}{(1+s^2)^{(|m|/2+\alpha_0/2+1)}} \left(1 - \frac{\alpha_0+1}{|m|+1} s^2\right) \quad (n=1), \tag{B 12b}$$

$$\underline{p}^{(0)} = \frac{s^{|m|}}{(1+s^2)^{(|m|/2+\alpha_0/2+2)}} \left(1 - \frac{\alpha_0+2}{|m|+1} s^2 + \frac{(\alpha_0+1)(\alpha_0+2)}{(|m|+1)(|m|+2)}\right) s^4 \quad (n=2). \tag{B 12c}$$

From either of these forms, it is clear that the eigenfunctions behave, as $s \to \infty$, as $s^{-\alpha_0}$, which is the expected behaviour for inviscid modes according to the discussion in § 3.1.

Up to this point, our results are in complete agreement with those derived by LBP in the inviscid framework. To describe the effect of viscosity, we must consider the next order of the expansion of (3.8) in powers of $\underline{k}^{-1}$, which gives:

$$\begin{aligned}(s^2+1)^2 \Delta_m \underline{p}^{(1)} - 8\left(s^2 + 1 - \frac{1}{C}\right)\underline{p}^{(1)} = {} & -\mathrm{i}\frac{D}{C}\left(2(s^2+1)\Delta_m \underline{p}^{(0)} - 8\underline{p}^{(0)}\right) \\ & + \frac{1}{2}\frac{m}{C^2}\left((s^2+1)\Delta_m^2 \underline{p}^{(0)} + \Delta_m (s^2+1)\Delta_m \underline{p}^{(0)} - 8\Delta_m \underline{p}^{(0)}\right)\end{aligned} \tag{B 13}$$

This equation defines a differential equation for $\underline{p}^{(1)}$ similar to that obtained for $\underline{p}^{(0)}$ at the lowest order, with a forcing term, defined in terms of $\underline{p}^{(0)}$, on the right-hand side. To obtain a well-behaved solution, the left-hand side must be orthogonal to the homogeneous solution of the equation. This condition determines the values of the coefficient $D(m, n)$. The derivation is standard, and leads to the general expression:

$$D(m,n) = \frac{m}{2C(m,n)} \frac{\displaystyle\int_0^\infty \frac{\underline{p}^{(0)}}{(1+s^2)^2}\left((s^2+1)\Delta_m^2 \underline{p}^{(0)} + \Delta_m(s^2+1)\Delta_m \underline{p}^{(0)} - 8\Delta_m \underline{p}^{(0)}\right) s\,\mathrm{d}s}{\displaystyle\int_0^\infty \frac{\underline{p}^{(0)}}{(1+s^2)^2}\left(2(s^2+1)\Delta_m \underline{p}^{(0)} - 8\underline{p}^{(0)}\right) s\mathrm{d}s}. \tag{B 14}$$

The integrals appearing in this expression can be evaluated analytically (Abramowitz & Stegun 1965). Here, we give the expression only for the first mode of the family, with $n = 0$:

$$D(m,0) = \frac{|m|(|m|+1)\mu_0^2(2\mu_0 + 1 - |m|)\left((2+|m|)\mu_0^2 + (7+2|m|)\mu_0 + 6\right)}{2(2\mu_0+3)(|m|\mu_0 + \mu_0 + 2)}, \tag{B 15}$$

with $\mu_0 = (\sqrt{m^2+8} + |m|)/2$. Similar expressions can be obtained for higher values of n, but are much more intricate.

Numerical values of $C(m, n)$ and $D(m, n)$ for $m = -1, -2, -3$ and $n = 0, 1, 2$ are given in table 5. Note that for $m < 0$, the coefficients $C(m, n)$ and $D(m, n)$ are always

$C(-1,0)=0.3333$	$(=1/3)$	$D(-1,0)=13.714$	$(=96/7)$
$C(-1,1)=0.1667$	$(=1/6)$	$D(-1,1)=72$	$(=72)$
$C(-1,2)=0.1$	$(=1/10)$	$D(-1,2)=219.74$	$(=16\,920/77)$
$C(-2,0)=0.1962$	$(=2/(5+3\sqrt{3}))$	$D(-2,0)=76.34$	
$C(-2,1)=0.1132$	$(=2/(9+5\sqrt{3}))$	$D(-2,1)=296.6$	
$C(-2,2)=0.0737$	$(=2/(15+7\sqrt{3}))$	$D(-2,2)=776.1$	
$C(-3,0)=0.1231$	$(=1/(4+\sqrt{17}))$	$D(-3,0)=274.4$	
$C(-3,1)=0.0875$	$(=4/(21+6\sqrt{17}))$	$D(-3,1)=862.2$	
$C(-3,2)=0.0548$	$(=1/(10+2\sqrt{17}))$	$D(-3,2)=2001.1$	

TABLE 5. Coefficients $C(m,N)$ and $D(m,N)$ for the lowest values of m and N.

positive. Results for $m>0$ can be deduced from the relations $C(-m,n)=C(m,n)$ and $D(-m,n)=-D(m,n)$.

Let us consider in more detail the structure of the 'inviscid solution' $\underline{p}^{(0)}$ given by (B 6) and (B 12). Because of to the factor $(1+s^2)^{-\mu}$, this solution is singular when $s^2=-1$. When $\underline{k}<0$, the change of variables defined by (B 4) leads to positive values of s^2 when r is real, so singularities do not occur on the real axis. In this case, the modes are regular. On the other hand, if $\underline{k}>0$, a singular point is found on the real r-axis, and occurs at the position $\underline{r}_c=\sqrt{-2C\underline{k}/m}$. This situation leads to the prediction of inviscid singular modes. Such modes were discarded by LBP, who concluded that inviscid centre modes exist only for negative k. However, it is shown in § 3.3 that centre modes of the present type are actually reached as a limit by some branches computed with the scaling of § 3. Note that modes with a similar structure were also found by SNB for the swirling Poiseuille flow.

Technically, there are two ways of justifying the continuation of the eigenmode structure through this critical layer. The first way would be to introduce the viscosity in a region neighbouring the singularity called the critical layer, and to solve an inner problem whose solution should be matched to the outer singular expression for (B 6). This argument was carried out by SNB in a related case. In the present case, it can be expected that the width of the critical layer is of order $\underline{r}-\underline{r}_c=O(\underline{k}^{-1/3})$ (or $r-r_c=O(Re^{-1/3})$ in primitive variables). Alternatively, we may argue that since $\underline{\omega}$ has a small positive imaginary part, the critical point $\underline{r}_c$ is actually slightly below (resp. above) the real axis for $m>0$ (resp. $m<0$). This is consistent with the rule given in Olendraru *et al.* (1999) which states that the contour of integration must lie above (resp. below) the critical point for $m>0$ (resp. $m<0$).

Appendix C. The inviscid centre modes in the region of the upper neutral curve

As for in the long-wave range, we consider the inviscid limit for centre modes in the vicinity of the 'upper neutral curve' by letting $\bar{k}\to\infty$ in the reduced equation (5.8). We consider the following expansion for the frequency and eigenmode:

$$\bar{\omega}=C_1\bar{k}+\frac{\mathrm{i}D_1}{\bar{k}}+O(\bar{k}^{-3}), \tag{C 1}$$

$$\bar{p}=\bar{p}^{(0)}+\bar{k}^{-2}\bar{p}^{(1)}. \tag{C 2}$$

It is also convenient to introduce a new variable s, defined in terms of $\bar{r}$ as follows:

$$s^2=\frac{m(2-Q)\bar{r}^2}{2C_1\bar{k}}. \tag{C 3}$$

Introducing this ansatz into (5.8) and retaining only the leading-order term leads to the following compact equation:

$$(s^2+1)^2\Delta_m\bar{p}^{(0)} - \frac{8Q}{Q-2}(s^2+1)\bar{p}^{(0)} - \frac{16L}{m(Q-2)^2}s^2\bar{p}^{(0)} - \frac{8}{(Q-2)C_1}\bar{p}^{(0)} = 0. \quad \text{(C 4)}$$

This equation is similar to the one obtained in the long-wave region. It admits a solution in terms of the hypergeometric function F with the following form:

$$\bar{p}^{(0)} = s^{|m|}(1+s^2)^{-\mu}F(a_1, b_1; |m|+1; -s^2); \quad \text{(C 5)}$$

with

$$\mu(\mu+1) = -\frac{2}{(Q-2)C} + Y/4, \quad \text{(C 6)}$$

$$a_1 = -\mu + \frac{|m|-\alpha_1}{2}, \quad \text{(C 7)}$$

$$b_1 = -\mu + \frac{|m|+\alpha_1}{2}, \quad \text{(C 8)}$$

$$Y = \frac{16L}{m(Q-2)^2}, \quad \text{(C 9)}$$

$$\alpha_1^2 = m^2 + \frac{8Q}{Q-2} + Y. \quad \text{(C 10)}$$

If $\alpha_1^2 \geqslant 0$, imposing $b_1 = -n$ allows us to obtain a bounded solution. This leads directly to the following expression for C_1:

$$C_1(m, n; Q, L) = \frac{8}{2-Q}\frac{1}{(|m|+\alpha_1+2n)(|m|+\alpha_1+2n+2)+Y}. \quad \text{(C 11)}$$

On the other hand, in the 'forbidden interval' defined by $\alpha_1^2 < 0$, the asymptotic behaviour of (C 5) has the form $\bar{p}^{(0)} \approx \sin(|\alpha_1|\log s + \phi)$, and no condition can lead to a bounded solution. This confirms that inviscid centre modes do not exist in this case.

For $\alpha_1^2 > 0$, the term $D_1(m, n)$ can be computed in the same way as was done in the long-wave range. The result is as follows:

$$D_1 = \frac{m}{2C_1}\frac{\displaystyle\int_0^\infty \frac{\bar{p}^{(0)}}{(1+s^2)^2}\left((s^2+1)\Delta_m\bar{p}^{(0)} + \Delta_m(s^2+1)^2\bar{p}^{(0)} - 8\frac{Q+1}{Q-2}\Delta_m\bar{p}^{(0)}\right)s\,\mathrm{d}s}{\displaystyle\int_0^\infty \frac{\bar{p}^{(0)}}{(1+s^2)^2}\left(2(s^2+1)\Delta_m\bar{p}^{(0)} - \frac{8Q}{Q-2}\bar{p}^{(0)}\right)s\,\mathrm{d}s}. \quad \text{(C 12)}$$

Again, the integrals appearing in this expression can be worked out analytically, leading, for the first mode of the family, to

$$D_1(m, 0) = \frac{-(Q-2)^2|m|(|m|+1)\mu_1^2(2\mu_1+1-|m|)}{2(2\mu_1+3)((Q-2)(|m|+1)\mu_1+2Q)} \times \big((2+|m|)(Q-2)\mu_1^2 + (2|m|(Q-2)+7Q-8)\mu_1 + 6Q\big), \quad \text{(C 13)}$$

with $\mu_1 = (\alpha_1 + |m|)/2$.

Note that, unlike in the previous section, these coefficients are not universal, but depend on the base flow parameters Q and L. Moreover, the predictions are valid only outside of the 'forbidden interval'. In the case $L = 0$, the term C_1 is positive

below the forbidden interval (i.e. for $Q \leqslant Q_c = 2m^2/(m^2+8)$), and negative above it (i.e. for $Q > 2$). The term D_1 is always negative. This means that the present analysis leads to stable regular modes on the 'stable' side of the neutral curve (for $k > -m/q$), and to unstable singular modes (i.e. with a critical layer) on the 'unstable' side of the neutral curve (for $k < -m/q$).

Finally, we give the limiting form of expressions (C 11) and (C 13) obtained for some particular values of Q (with, again, $L = 0$).

(i) $Q = 0$

This case corresponds to the swirling Poiseuille flow already investigated by SNB. In this case we have:

$$C_1(m,n) = \frac{1}{(|m|+n)(|m|+n+1)}, \tag{C 14}$$

$$D_1(m,0) = \frac{2m^2(|m|+1)(|m|+2)^2}{2|m|+3}. \tag{C 15}$$

These results correspond, respectively, to expressions (3.24) and (3.27) of SNB (except that a different notation is used).

(ii) $Q = Q_c = 2m^2/(m^2+8)$

This value corresponds to the lower bound of the 'forbidden interval'. It is found that in this case the analysis is still valid, and leads to the following predictions:

$$C_1(m,n) = \frac{m^2}{\big(|m|+2n\big)\,\big(|m|+2n+2\big)}, \tag{C 16}$$

$$D_1(m,0) = \frac{-8|m|^3(|m|+1)(m^2+12|m|+32)}{(m^2+8)^2(|m|+2)(|m|+3)}. \tag{C 17}$$

(iii) $Q \to 2^+$

This is the upper bound of the 'forbidden interval'. In this limit, the terms C_1 and D_1 have the following behaviour:

$$C_1(m,n) \approx -\frac{1}{2} + \frac{|m|+1+2n}{4}\sqrt{Q-2} + O(Q-2), \tag{C 18}$$

$$D_1(m,0) \approx -6|m|(1+|m|)\sqrt{Q-2} + O(Q-2). \tag{C 19}$$

(iv) $Q \to \infty$

$$C_1(-m,n) \approx -Q^{-1}C(m,n), \tag{C 20}$$

$$D_1(-m,n) \approx -Q^2 D(m,n), \tag{C 21}$$

where $C(m,n)$ and $D(m,n)$ are the expressions for the long-wave centre modes given in the previous section. As expected, in this limit, the results in the region of the upper curve become equivalent to those in the long-wave range.

REFERENCES

Abramowitz, M. & Stegun, I. A. 1965 *Handbook of Mathematical Functions*. Dover.

Bajer, K., Bassom, A. P. & Gilbert, A. D. 2001 Accelerated diffusion in the centre of a vortex. *J. Fluid Mech.* **437**, 395–711.

Batchelor, G. K. 1964 Axial flow in trailing line vortices. *J. Fluid Mech.* **20**, 645–658.

Bender, C. & Orszag, S. 1978 *Advanced Mathematical Methods for Scientits and Engineers*. McGraw-Hill.

Briggs, R. J., Daugherty, J. D. & Levy, R. H. 1970 Role of Landau damping in crossed-field electron beams and inviscid shear flows. *Phys. Fluids* **13** (2), 421–432.

Fabre, D. & Jacquin, L. 2004 Viscous instabilities in trailing vortices at large swirl number. *J. Fluid Mech.* **500**, 239–262.

Fabre, D., Sipp, D. & Jacquin, L. 2006 Kelvin waves and the singular modes of the Lamb–Oseen vortex. *J. Fluid Mech.* **551**, 235–274.

Heaton, C. J. 2007 Centre modes in inviscid vortex flows, and their application to the stability of the Batchelor vortex. *J. Fluid Mech.* **576**, 325–348.

Le Dizés, S. & Lacaze L. 2005 An asymptotic descriptions of vortex Kelvin modes. *J. Fluid Mech.* **542**, 69–96.

Le Dizès, S. & Fabre, D. 2007 Large-Reynolds-number asymptotic analysis of viscous centre modes in vortices. *J. Fluid Mech* **585**, 153–180.

Leibovich, S. & Stewartson, K. 1983 A sufficient condition for the instability of columnar vortices. *J. Fluid Mech.* **126**, 335–356.

Leibovich, S., Brown, S. & Patel, Y. 1986 Bending waves on inviscid columnar vortices. *J. Fluid Mech.* **173**, 595–624.

Mayer, E. W. & Powell, K. G. 1992 Viscous and inviscid instabilities of a trailing vortex. *J. Fluid Mech.* **245**, 91–114.

Olendraru, C., Sellier, A., Rossi, M. & Huerre, P. 1999 Inviscid instability of the Batchelor vortex: absolute–convective transitions and spatial branches. *Phys. Fluids* **11** (7), 1805–1820.

de Souza, M. O. 1998 Instabilities of rotating and unsteady flows. PhD thesis, University of Cambridge, UK.

Stewartson, K. & Brown, S. 1985 Near-neutral centre-modes as inviscid perturbations to a trailing line vortex. *J. Fluid Mech.* **156**, 387–399.

Stewartson, K. & Capell, K. 1985 On the stability of ring modes in a trailing line vortex: the lower neutral points. *J. Fluid Mech.* **156**, 369–386.

Stewartson, K. & Leibovich, S. 1987 On the stability of a columnar vortex to disturbances with large azimuthal wavenumbers : the upper neutral points. *J. Fluid Mech.* **178**, 549–566.

Stewartson, K., Ng, T. W. & Brown, S. 1988 Viscous centre modes in the stability of swirling Poiseuille flow. *Phil. Trans. R. Soc. Lond.* A **324**, 473–512.